THE JOURNAL OF BIOLOGICAL CHEMISTRY VOL. 286, NO. 2, pp. 1445–1452, January 14, 2011

Partial Biopterin Deficiency Disturbs Postnatal Development of the Dopaminergic System in the Brain*[S]

Received for publication, June 29, 2010, and in revised form, October 29, 2010 Published, JBC Papers in Press, November 9, 2010, DOI 10.1074/jbc.M110.159426

Daigo Homma[‡], Chiho Sumi-Ichinose[§], Hirofumi Tokuoka[‡], Kazuhisa Ikemoto[§], Takahide Nomura[§], Kazunao Kondo[§], Setsuko Katoh[¶], and Hiroshi Ichinose[‡1]

From the [‡]Graduate School of Bioscience and Biotechnology, Tokyo Institute of Technology, Yokohama 226-8501, Japan, the [§]Department of Pharmacology, Fujita Health University School of Medicine, Toyoake 470-1192, Japan, and the [¶]Meikai University School of Dentistry, Sakado, Saitama 350-0283, Japan

Postnatal development of dopaminergic system is closely related to the development of psychomotor function. Tyrosine hydroxylase (TH) is the rate-limiting enzyme in the biosynthesis of dopamine and requires tetrahydrobiopterin (BH4) as a cofactor. To clarify the effect of partial BH4 deficiency on postnatal development of the dopaminergic system, we examined two lines of mutant mice lacking a BH4-biosynthesizing enzyme, including sepiapterin reductase knock-out (*Spr*$^{-/-}$) mice and genetically rescued 6-pyruvoyltetrahydropterin synthase knock-out (*DPS-Pts*$^{-/-}$) mice. We found that biopterin contents in the brains of these knock-out mice were moderately decreased from postnatal day 0 (P0) and remained constant up to P21. In contrast, the effects of BH4 deficiency on dopamine and TH protein levels were more manifested during the postnatal development. Both of dopamine and TH protein levels were greatly increased from P0 to P21 in wild-type mice but not in those mutant mice. Serotonin levels in those mutant mice were also severely suppressed after P7. Moreover, striatal TH immunoreactivity in *Spr*$^{-/-}$ mice showed a drop in the late developmental stage, when those mice exhibited hind-limb clasping behavior, a type of motor dysfunction. Our results demonstrate a critical role of biopterin in the augmentation of TH protein in the postnatal period. The developmental manifestation of psychomotor symptoms in BH4 deficiency might be attributable at least partially to high dependence of dopaminergic development on BH4 availability.

Tetrahydrobiopterin (BH4)[2] is an essential cofactor for phenylalanine hydroxylase (PAH, EC 1.14.16.2), tyrosine hydroxylase (TH, EC 1.14.16.3) and tryptophan hydroxylase (EC, 1.14.16.4). TH and tryptophan hydroxylase are essential for synthesizing dopamine and serotonin, respectively, whereas PAH is necessary for maintaining the proper phenylalanine concentration. Defects in the biosynthesis of BH4 can result in malfunctions of various organs, including the brain, due to insufficient activity of the aforementioned hydroxylases.

BH4 is biosynthesized from GTP by three enzymes, including GTP cyclohydrolase 1 (GCH1, EC 3.5.4.16), 6-pyruvoyltetrahydropterin synthase (PTS, EC 4.2.3.12), and sepiapterin reductase (SPR, EC 1.1.1.153) (1). Mutations in the genes for these proteins cause biopterin deficiency with or without hyperphenylalaninemia in humans, leading to decreased levels of monoamine neurotransmitters (2).

We and other groups have generated transgenic mice that are defective in the genes for BH4 biosynthesis. *Pts* homozygous knock-out mice (*Pts*$^{-/-}$) are born without obvious morphological abnormality but die within 2 days after birth (3, 4). *Spr*$^{-/-}$ mice are also born normal. In contrast to *Pts*$^{-/-}$ mice, *Spr*$^{-/-}$ mice can survive for a few weeks with growth retardation (5, 6), possibly due to the alternative pathway for SPR by aldo-keto reductases and carbonyl reductases (7, 8). We have demonstrated that the amount of TH protein is reduced in mutant mice, especially in nerve terminals, due to biopterin deficiency.

Monoamine deficiency in patients with biopterin deficiency results in a variety of clinical manifestations with typical onset from neonate to childhood. Dopa-responsive dystonia (DYT5) shows a partial biopterin deficiency caused by a dominant mutation in the *GCH1* gene (9, 10), and its symptoms of dystonia appear mostly in childhoods but not in the neonatal period, whereas parkinsonism appears later in life only in a subset of patients. Some patients with SPR deficiency show similar age-dependent alterations in clinical symptoms (11). These symptoms are well responsive to the L-DOPA treatment and thought to be caused by dysfunction of the nigrostriatal dopaminergic system due to insufficient production of dopamine in the striatum (12, 13). However, it is poorly understood why dystonia appears in childhood but not in the neonatal period. To understand the molecular mechanisms underlying the DYT5 pathology, it is crucial to systematically examine how BH4 deficiency affects the development of brain, especially monoaminergic systems, using model animals.

Here, using *Spr*$^{-/-}$ and *DPS-Pts*$^{-/-}$ mice (*i.e. Pts*$^{-/-}$ mice with genetically rescued noradrenaline-producing cells) (14), we investigated the effect of biopterin deficiency on postnatal

* This work was supported by grants-in-aid for Scientific Research from the Ministry of Education, Culture, Sports, Science, and Technology of Japan, by Health and Labor Sciences Research Grants for Research on Intractable Diseases from the Ministry of Health, Labor, and Welfare of Japan, and by the Japan Science and Technology Agency, CREST (21500305 and 22090250).

[S] The on-line version of this article (available at http://www.jbc.org) contains supplemental Fig. 1.

[1] To whom correspondence should be addressed: Graduate School of Bioscience and Biotechnology, Tokyo Institute of Technology, 4259-B7, Nagatsuta, Yokohama 226-8501, Japan. Fax: 81-45-924-5807; E-mail: hichinos@bio.titech.ac.jp.

[2] The abbreviations used are: BH4, tetrahydrobiopterin; AADC, aromatic L-amino acid decarboxylase; GCH1, GTP cyclohydrolase 1; PAH, phenylalanine hydroxylase; PTS, 6-pyruvoyltetrahydropterin synthase; SPR, sepiapterin reductase; TH, tyrosine hydroxylase; ANOVA, analysis of variance.

regulation of monoamine metabolism in the brain. We found that wild-type mice exhibited a marked up-regulation of both dopamine and TH protein levels in parallel and that partial BH4 deficiency in both *Spr*$^{-/-}$ and *DPS-Pts*$^{-/-}$ mice disturbed the developmental up-regulation of dopamine and TH protein levels. *Spr*$^{-/-}$ mice showed milder dystonic hind-limb clasping at P14 compared with that observed in *DPS-Pts*$^{-/-}$ mice. Our data demonstrate the importance of biopterin levels for postnatal development of the dopaminergic system in the brain.

EXPERIMENTAL PROCEDURES

Animals—*Spr* heterozygous mutant mice were obtained from Lexicon Pharmaceuticals Inc. (Woodlands, TX) (5) and crossed with C57Black/6J mice for more than 10 generations. *DPS-Pts*$^{-/-}$ mice were generated as previously described (14). All animal experiments were carried out in accordance with the general guidelines for animal experiments in Tokyo Institute of Technology and Fujita Health University. Littermate wild-type mice were used as controls.

Biochemical Analysis—Mice were sacrificed by cervical dislocation, and tissues were immediately dissected out. The tissues from *Spr*$^{+/+}$ and *Spr* mutant mice were homogenized with 20 mM sodium phosphate buffer (pH 7.4) containing 0.1 mM EDTA, 1 mM ascorbic acid, 1 mM *N*-acetylcysteine, and 10% glycerol and centrifuged at 20,400 × *g* for 10 min. For the Western blot assay, dithiothreitol was added to an aliquot at a final concentration of 1 mM and kept frozen at −80 °C until analysis. For BH4, monoamine, and amino acid measurements, another aliquot was deproteinized by 0.2 M perchloric acid and centrifuged at 15,000 × *g* for 20 min. Aliquots of the supernatant were used for analyses as previously described (5). Tissue homogenates from *Pts*$^{+/+}$ and *Pts* mutant mice were prepared and subjected to biochemical analyses as previously described (4). To measure total biopterin contents, pteridines in the supernatant were oxidized by adding 1 M HCl containing 1% I_2 and 2% KI for 1 h at room temperature and then subjected to HPLC analyses (4). Amino acid content in the brain was measured by an L-8500 amino acid analyzer (Hitachi, Tokyo, Japan).

Western Blotting—Tissue homogenates were subjected to Western blot analysis. In brief, protein from brain or liver homogenates was separated by 10% SDS-polyacrylamide gel electrophoresis, blotted onto a polyvinylidene difluoride membrane (Bio-Rad), blocked with 5% skim milk, incubated with anti-TH antibody (1:3,000 or 1:5,000; Millipore AB152, MA), anti-aromatic L-amino acid decarboxylase (AADC: EC 4.1.1.28) antiserum (1:5,000) (4), anti-PAH antibody (1:2,000; Calbiochem OP71L, CA), anti-GCH1 antiserum (1:5,000) (15), or anti-β-actin antibody (Sigma A5441, 1:30,000 or 1:10,000 for the analyses of *Spr* or *Pts* mutant mice, respectively), and then incubated with horseradish peroxidase-conjugated anti-rabbit IgG (GE Healthcare NA9310) or anti-mouse IgG (GE Healthcare NA9340). Immunoreactivity was detected using Immobilon Western chemiluminescent HRP substrate (Millipore) for analyses of *Spr* mutant mice or ECL-Plus (GE Healthcare) for analyses of *Pts* mutant mice.

Immunohistochemical Analysis—Mice were anesthetized with diethyl ether and transcardially perfused with ice-cold 0.9% NaCl followed by 4% paraformaldehyde in 0.1 M phosphate buffer (pH 7.4). Coronal brain slices (30 μm thick) were incubated in HistoVT one (Nakarai Tesque, Kyoto, Japan) at 70 °C for 20 min followed by incubation in 1% H_2O_2 in PBS and blocking with 5% pig serum. Slices were then incubated overnight with anti-TH antibody (1:10,000; Millipore), anti-AADC antiserum (1:10,000) or anti-μ-opioid receptor antibody (1:2,000; Millipore AB1774). Slices were then incubated with biotin-conjugated secondary antibodies, anti-rabbit IgG (1:250; Vector Laboratories BA-1000, CA), or anti-guinea pig IgG (1500; Vector BA-7000) and further processed with Elite ABC kit. Visualization was performed in PBS containing 0.02% diaminobenzidine and 0.002% H_2O_2.

Analysis of Hind-limb Clasping—To quantify hind-limb clasping, P14 mice were picked up from the cage and suspended by the tail for 25 s while being videotaped. The video was analyzed, and the duration of hind-limb clasping near the body was evaluated for each mouse. Clasping events lasting less than 0.5 s were excluded from the analysis because mice occasionally cross their legs as an escape behavior.

Statistical Analysis—All data were expressed as the mean ± S.E. For the HPLC and Western blotting data, multiple comparisons were performed using a one-way ANOVA followed by a Tukey's post hoc test. For the behavioral data, multiple comparisons were performed using a Kruskal-Wallis nonparametric one-way ANOVA followed by a Steel-Dwass post hoc test.

RESULTS

BH4 and Monoamine Contents in the Brain of BH4-deficient Mice—To evaluate how genetic deletion of the *Spr* gene alters BH4 and monoamine contents in the brains at early postnatal stages, we biochemically analyzed *Spr*-mutant mice at postnatal day 0 (P0), P7, and P14. Wild-type and heterozygous *Spr*-mutant mice showed no significant difference in BH4 content from P0 to P14 (Fig. 1*A*). BH4 content in the brains of *Spr*$^{-/-}$ mice was significantly lower than wild-type mice at all time points examined: 26.1% at P0, 19.6% at P7, and 24.8% at P14 (Fig. 1*A*). More than 90% of the total biopterin was present in a tetrahydro form, as BH4, in most of the brains examined.

We next measured the contents of the monoamine neurotransmitters and their metabolites in the brain to elucidate the effect of low biopterin availability on the biosynthesis of the neurotransmitters in an early postnatal stage. In wild-type and heterozygous *Spr*-mutant mice, we found a marked increase in dopamine content with postnatal days (in wild-type mice and 3.9 ± 2.0, 8.9 ± 1.2, and 14.6 ± 3.1 pmol/mg of protein at P0, P7, and P14, respectively). The elevation in dopamine content may reflect the postnatal maturation of the dopaminergic system in mice. Dopamine content in the brains of *Spr*$^{-/-}$ mice was ~50% that of wild-type mice at P0; however, there was no statistical difference between wild-type and *Spr*$^{-/-}$ mice ($p = 0.802$). Unlike the wild-type mice, *Spr*$^{-/-}$ mice showed almost no elevation in dopamine content, even at P7 or P14 (Fig. 1*B*). As a result, the dopamine deficiency in

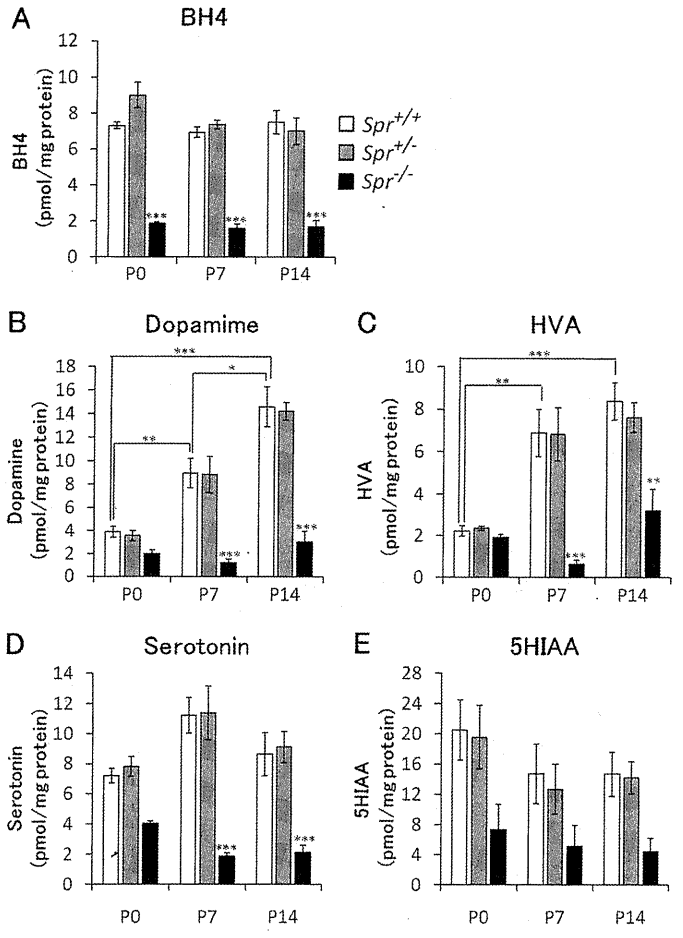

FIGURE 1. **Alternation of BH4 and monoamine contents in the brains of wild-type and *Spr* mutant mice in the early postnatal period.** Contents of BH4 (*A*), dopamine (*B*), homovanillic acid (*HVA*, *C*), serotonin (*D*), and 5-hydroxyindoleacetic acid (*5HIAA*, *E*) in whole brain homogenates were measured by HPLC with fluorescence (*A*) or electrochemical (*B–E*) detection. The values represent the mean ± S.E. $n = 4$ mice for all groups. *, $p < 0.05$; **, $p < 0.01$; ***, $p < 0.001$, one-way ANOVA followed by Tukey's test. *Stars over bars* indicate difference between wild-type and $Spr^{-/-}$ mice within the same age, and *stars above lines* indicate difference between wild-type mice of different ages.

$Spr^{-/-}$ mice compared with wild-type mice was more severe at P7 and P14. The level of homovanillic acid, a main metabolite of dopamine, in the brains of $Spr^{-/-}$ mice was almost the same as the level in wild-type mice at P0 (Fig. 1*C*: 87.1% of wild-type mice), which was much milder than at P7 or P14. These results indicate that a dopamine deficiency in $Spr^{-/-}$ mice becomes more prominent with postnatal development.

Similarly, serotonin content in the brains of $Spr^{-/-}$ mice was moderately decreased at P0 (56% of wild-type) and was not further increased at P7 and P14 (Fig. 1*D*). The content of 5-hydroxylindoleacetic acid, a serotonin metabolite, in $Spr^{-/-}$ mice was decreased to 36% that of wild type at P0 (Fig. 1*E*).

We further investigated the alterations in the contents of biopterin, monoamines, and their metabolites in the brain of *DPS-Pts*$^{-/-}$ mice, another model of partial biopterin deficiency. Using *DPS-Pts*$^{-/-}$ mice, we were able to analyze the late developmental stage because they can survive beyond weaning (14), whereas most $Spr^{-/-}$ mice die before P21 (5). Because *DPS*-gene does not influence the monoamine contents in wild-type mice (data not shown), we used littermate $Pts^{+/+}$ mice for the control in this study. We found that the level of biopterin was highest around P0-P7 and gradually decreased until P28 in wild-type mice (Fig. 2*A*). Biopterin levels in *DPS-Pts*$^{-/-}$ mice were ~30–40% that of wild-type levels (Fig. 2*A*). Dopamine levels peaked around P21 in wild-type mice, and similar to $Spr^{-/-}$ mice, there was almost no elevation in dopamine content in *DPS-Pts*$^{-/-}$ mice (Fig. 2*B*). Serotonin content in *DPS-Pts*$^{-/-}$ mice was similar to wild-type at P0 and dropped to ~10–20% that of the wild-type level after P7. Collectively, the results of *Spr* and *Pts* mutant mice demonstrated that partial biopterin deficiency prevented up-regulation of dopamine in the early developmental period.

Alteration in the TH Protein Level during a Developmental Period—Because we previously observed a great reduction in the amount of the TH protein in P17 $Spr^{-/-}$ mice and adult *DPS-Pts*$^{-/-}$ mice, we examined developmental alterations in the TH protein level from newborn to P14 in $Spr^{-/-}$ or P28 in *DPS-Pts*$^{-/-}$ mice as well as in wild-type mice. TH protein levels in brains of wild-type mice were markedly elevated from P0 to P14 (Fig. 3, *A*, *B*, and *D*), similar to the increase in dopamine content. In newborns, TH protein levels in $Spr^{-/-}$ mice were slightly lower than that in $Spr^{+/+}$ or $Spr^{+/-}$ mice (61% of levels in $Spr^{+/+}$ mice). Interestingly, the increase in TH protein levels observed in wild-type mice was strikingly impaired in $Spr^{-/-}$ (Fig. 3, *A* and *B*) and *DPS-Pts*$^{-/-}$ mice (Fig. 3*D*). In contrast, the AADC protein level was unchanged between P0 and P14 for all genotypes examined (Fig. 3, *A* and *C*).

Immunohistochemical Study of Striatal TH Expression $Spr^{-/-}$ mice—Because the Western blot analysis suggested that TH protein expression in the striatum may be developmentally affected in $Spr^{-/-}$ mice, we performed an immunohistochemical analysis for TH in the striatum. In wild-type mice, striatal TH immunoreactivity increased greatly from P0 to P21 (Fig. 4*A*). $Spr^{-/-}$ mice showed almost no increase in TH immunoreactivity, although the staining pattern at P0 was comparable with that in wild-type mice (Fig. 4*A*).

We also noticed that wild-type and $Spr^{-/-}$ mice showed a different developmental pattern of TH immunoreactivity between the striatal matrix and the striosome. In both genotypes, TH immunoreactivity in the striosome was stronger than that in the matrix at P14 (Fig. 4, *A* and *C*). In wild-type mice, matrix TH immunoreactivity increased later, and the boundary of the striosome and the matrix disappeared by P21 (Fig. 4, *A* and *C*). However, in $Spr^{-/-}$ mice, matrix TH immunoreactivity did not elevate after P7, and striosome TH immunoreactivity seemed to decrease after P14 (Fig. 4*A*), resulting in an overall reduction of TH immunoreactivity. We confirmed that these patchy compartments of TH immunoreactivity were mostly from the striosome by staining for the μ-opioid receptor, a marker for the striosome (Fig. 4*C*). Formation of striosome seemed to be unaffected in $Spr^{-/-}$ mice at P14 (Fig. 4*C*) and also at P21 (data not shown) judging from the staining pattern of μ-opioid receptor. These results suggest that *Spr* deficiency differently affects TH protein levels in the striosome and the matrix during postnatal development.

To verify normal projection of the nigral dopaminergic axons to the striatum, we stained striatal slices with the anti-

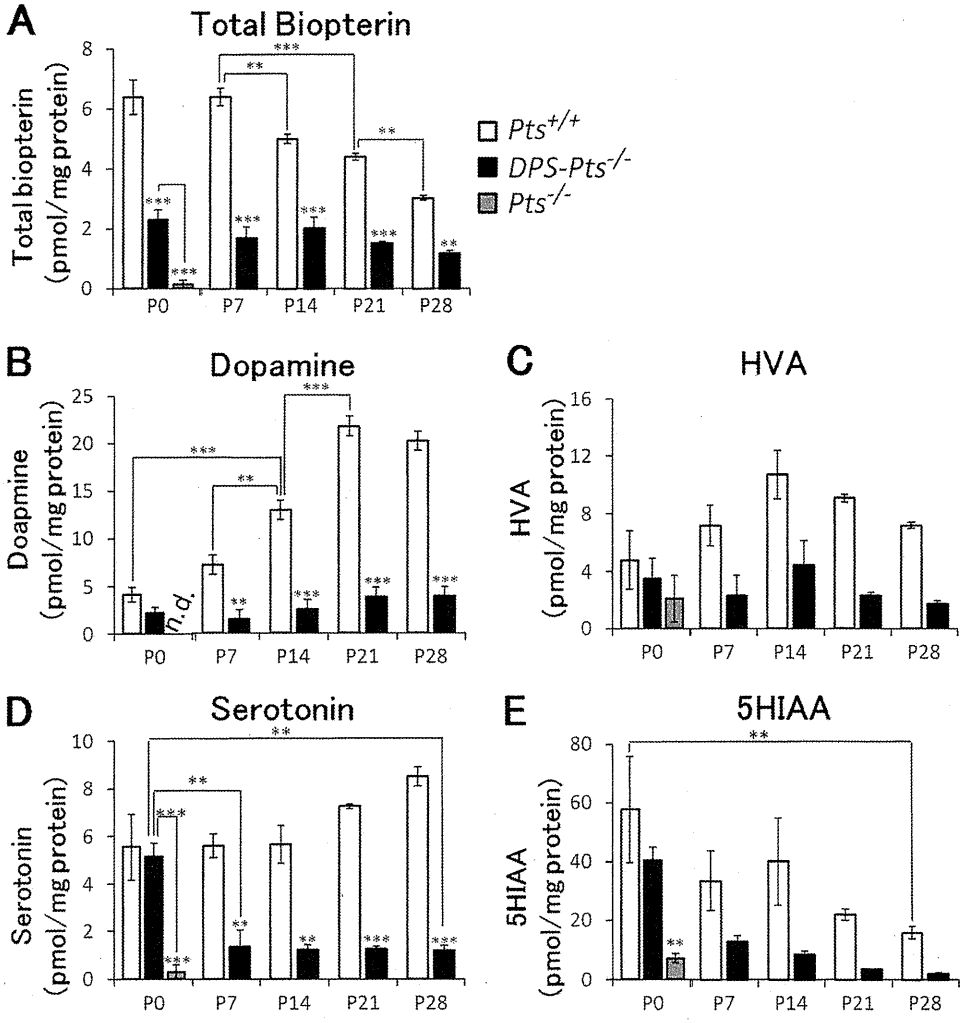

FIGURE 2. **Alternation of biopterin and monoamine contents in the brains of wild-type and *Pts* mutant mice in the early postnatal period.** Contents of total biopterin (*A*), dopamine (*B*), homovanillic acid (*HVA*, *C*), serotonin (*D*), and 5-hydroxyindoleacetic acid (*5HIAA*, *E*) in whole brain homogenates were measured by HPLC with fluorescence (*A*) or electrochemical (*B–E*) detection. Values represent the mean ± S.E. $n = 3$ mice for all groups. *, $p < 0.05$; **, $p < 0.01$; ***, $p < 0.001$, one-way ANOVA followed by Tukey's test. *Stars over bars* indicate differences between wild-type and *Pts* mutant mice within the same age, and *stars above lines* indicate differences between *DPS-Pts*$^{-/-}$ and *Pts*$^{-/-}$ mice or between wild-type or *DPS-Pts*$^{-/-}$ mice of different ages.

body against AADC, another marker for dopaminergic neurons in the striatum. As shown in Fig. 4*B*, AADC immunoreactivity was increased with development both in the wild-type and *Spr*$^{-/-}$ mice, suggesting that biopterin deficiency does not grossly affect the projection of nigrostriatal dopaminergiç neurons during postnatal development. Collectively, immunohistochemical analyses revealed that postnatal development of striatal TH protein expression is perturbed in the striatum of *Spr*$^{-/-}$ mice.

BH4 and BH4-related Enzymes in the Liver of Spr$^{-/-}$ *Mice*—We further explored the developmental effect of genetic deletion of the *Spr* gene on the BH4 content and expression levels of BH4-related enzymes in the liver, where metabolism of phenylalanine takes place. We first measured BH4 content in early postnatal stages. We found that BH4 content in the liver gradually increased from P0 to P14 in wild-type and heterozygous *Spr* mutant mice (Fig. 5*A*). Homozygous *Spr* mutant mice exhibited severely decreased levels of BH4, less than 5% at P0, P7, and P14 as compared with wild-type mice (Fig. 5*A*), whereas the amount of BH4 in the liver was similar to the amount in the brain (Fig. 1*A*), ~2 pmol/mg of protein.

In the brain, biopterin deficiency resulted in low TH protein levels, as described above. To evaluate whether the liver PAH protein level is similarly affected by biopterin deficiency, we examined the protein expression levels of PAH by Western blotting. PAH expression in wild-type mice was drastically increased during the postnatal period. In addition, *Spr*$^{-/-}$ mice showed a slight tendency toward reduced PAH protein levels, although the differences were not statistically significant (Fig. 5, *B* and *C*). In contrast, GCH1 expression was not altered in *Spr*$^{-/-}$ mice (Fig. 5, *B* and *D*). We confirmed the disappearance of the Spr protein in *Spr*$^{-/-}$ mice, whereas the expression level of Spr protein showed a developmental increase in wild-type mice (Fig. 5, *B* and *E*). These data highlight the severe impairment of the postnatal augmentation of TH protein levels in the brain.

Phenylalanine and Tyrosine Levels in the Brain of Biopterin-deficient Mice—Spr$^{-/-}$ and DPS-*Pts*$^{-/-}$ mice show hyperphenylalaninemia because biopterin content in the liver is low and leads to low PAH activity (5, 14). Because hyperphenylalaninemia can affect monoamine neurotransmitter metabolism in the brain, we next measured the contents of phenylala-

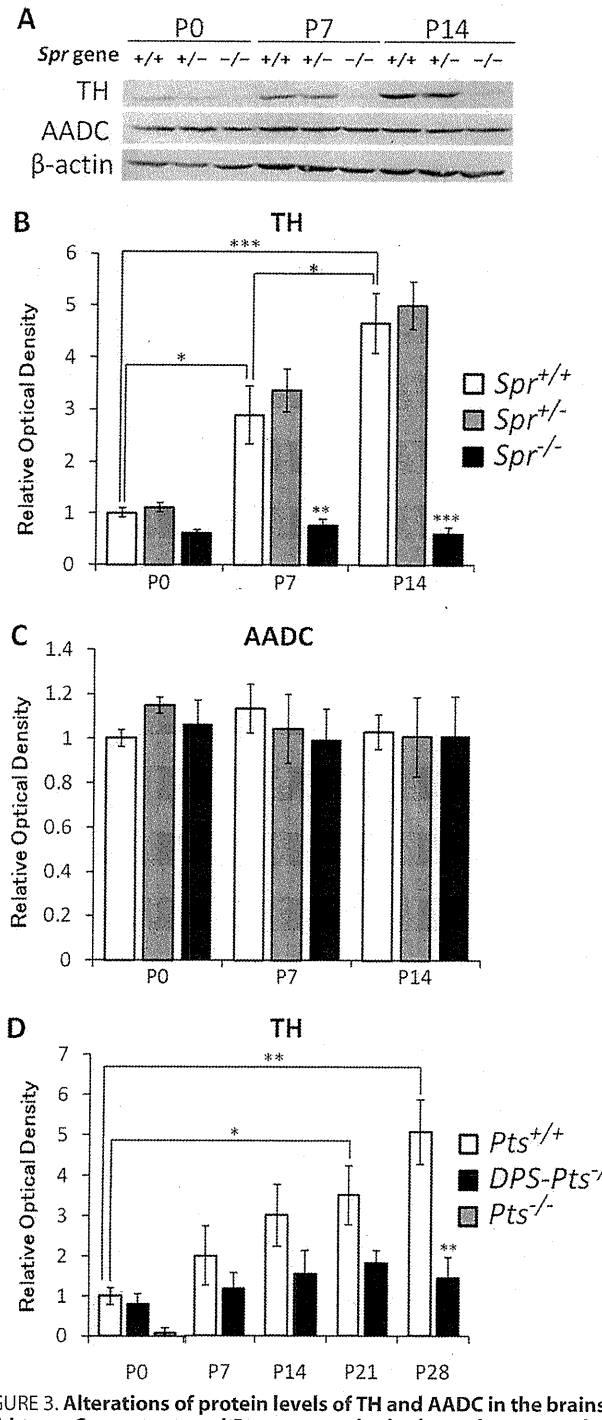

FIGURE 3. **Alterations of protein levels of TH and AADC in the brains of wild-type, *Spr* mutant, and *Pts* mutant mice in the early postnatal period.** *A*, 50 μg of protein from brain homogenates of wild-type and *Spr* mutant mice was separated by 10% SDS-PAGE and immunoblotted with specific antibodies against TH, AADC, and β-actin. *B* and *C*, shown is summary quantification of Western blot signals of TH (*B*) and AADC (*C*). *D*, shown is summary quantification of Western blot signals of TH. 30 μg of protein from the brain homogenates of wild-type and *DPS-Pts*$^{-/-}$ mice was separated by 10% SDS-PAGE and immunoblotted with specific antibodies against TH and β-actin. Quantified values of immunoblot signals were first normalized to β-actin immunoreactivity, and relative ratios to the mean value in P0 wild-type mice are shown. Values represent the mean ± S.E. $n = 4$ (*B* and *C*) or $n = 3$ (*D*) mice for all groups. *, $p < 0.05$; **, $p < 0.01$; ***, $p < 0.001$, one-way ANOVA followed by Tukey's test. *Stars over bars* indicate differences between wild-type and mutant mice within the same age, and *stars above lines* indicate differences between wild-type or mutant mice of different ages.

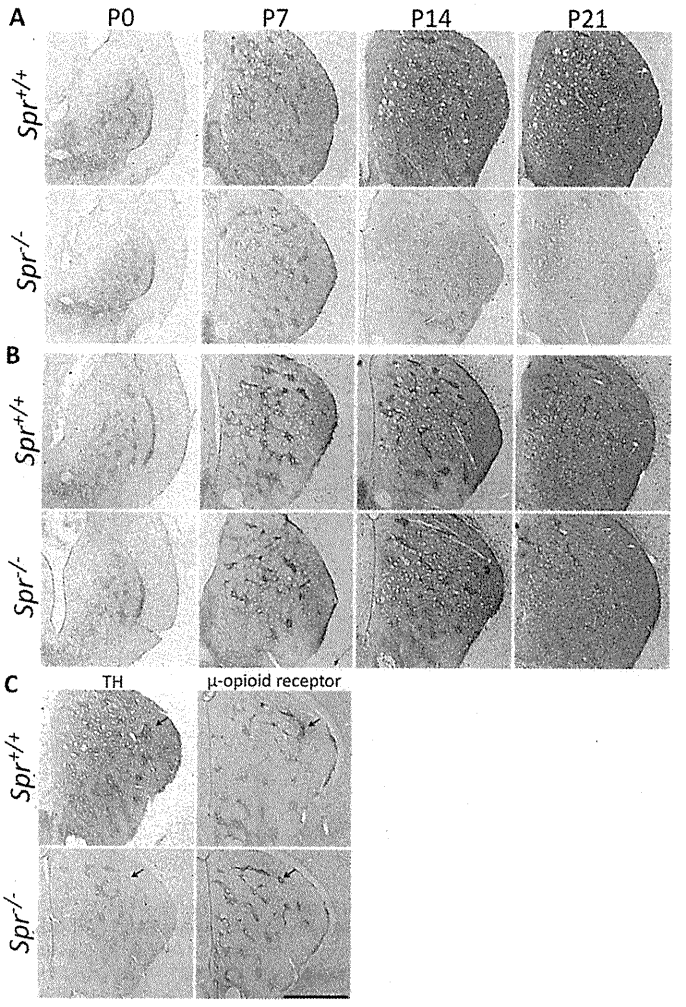

FIGURE 4. **Immunohistochemical analysis of postnatal development of the nigrostriatal dopaminergic system in *Spr* mutant mice.** Striata of *Spr*$^{+/+}$ and *Spr*$^{-/-}$ mice were immunostained with anti-TH antibody (*A*) and anti-AADC antiserum (*B*). Neighboring striatal sections of P14 mice were immunostained for TH and the μ-opioid receptor, a striosome marker (*C*). Patches of high TH immunoreactivity were colocalized with the striosome marker. *Scale bar*, 500 μm.

nine and tyrosine in the brains of biopterin-deficient mice. Both *Spr*$^{-/-}$ and *DPS-Pts*$^{-/-}$ mice showed drastically increased levels of phenylalanine at P7, but they were not severely affected at P0 (supplemental Fig. 1, *A* and *C*). Accumulation of phenylalanine was partially alleviated after P14 in both mutant mice (supplemental Fig. 1, *A* and *C*). Tyrosine content at P0 was significantly reduced in *Spr*$^{-/-}$ mice than in wild-type mice, and age-related decreases were observed for all genotypes (supplemental Fig. 1*B*). Tyrosine levels in *Spr*$^{-/-}$ and *DPS-Pts*$^{-/-}$ mice were lower than those in wild-type mice (supplemental Fig. 1, *B* and *D*).

Hind-limb Clasping in Spr$^{-/-}$ *Mice*—The nigrostriatal dopaminergic neurons play a critical role in coordination of voluntary movements. The loss of striatal TH protein and dopamine in *Spr*$^{-/-}$ mice may affect motor activity in the early postnatal period. To examine whether *Spr*$^{-/-}$ mice show any dystonic behavior, we performed the tail suspension test. We observed dystonic hind-limb clasping in *DPS-Pts*$^{-/-}$ mice (16), as shown in the transgenic mice expressing mutant torsinA, a model for DYT1 dystonia (17). *Spr*$^{-/-}$ mice

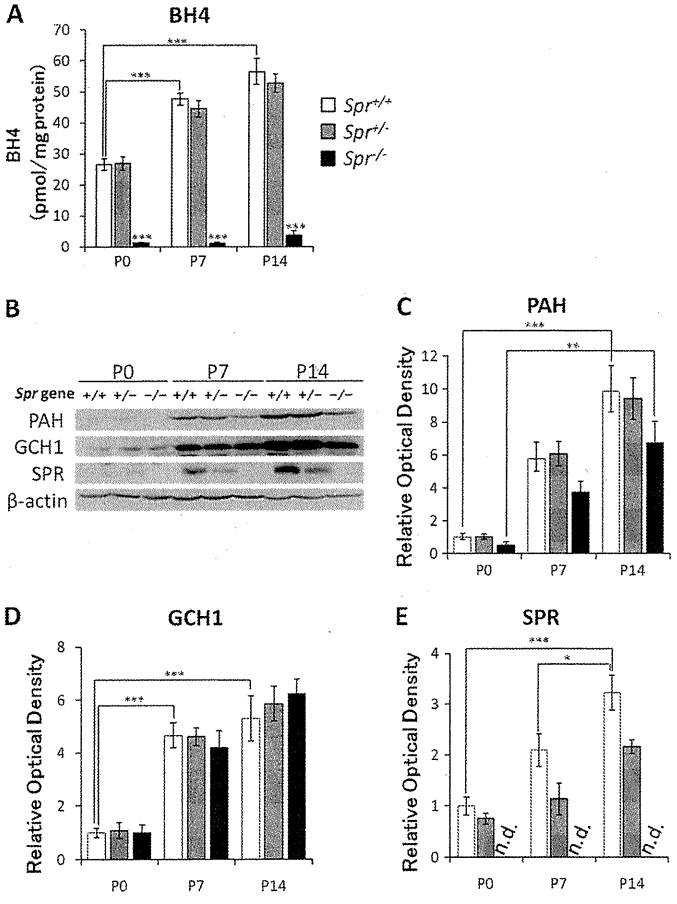

FIGURE 5. **Alternation of BH4 content and protein levels of PAH, GCH1, and SPR in the liver of *Spr* mutant mice in the early postnatal period.** *A*, BH4 content in the liver was measured at P0, P7, and P14. *B*, 50 μg of protein in the liver homogenate were separated by 10% SDS-PAGE and immunoblotted with specific antibodies against PAH, GCH1, SPR, and β-actin. *C–E*, shown is a summary quantification of Western blot signals of PAH (*C*), GCH1 (*D*), and SPR (*E*). Quantified values of immunoblot signals were first normalized to β-actin immunoreactivity, and relative ratios to the mean value in P0 $Spr^{+/+}$ mice are shown. Data represent the mean ± S.E. $n = 4$ mice for all groups. *, $p < 0.05$; **, $p < 0.01$; ***, $p < 0.001$, one-way ANOVA followed by Tukey's multiple comparison test. *Stars over bars* indicate differences between $Spr^{+/+}$ and $Spr^{-/-}$ mice within the same age, and *stars above lines* indicate differences between $Spr^{+/+}$ mice of different ages.

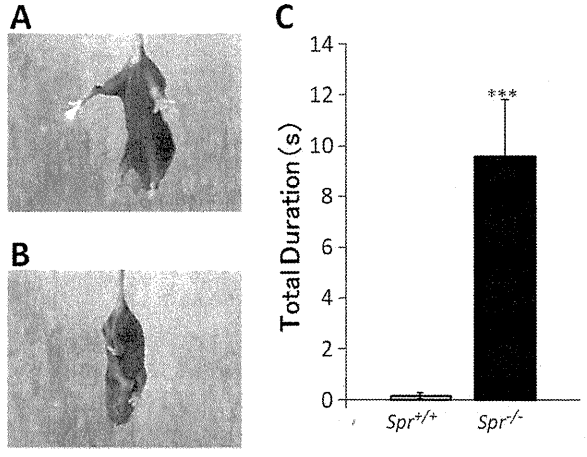

FIGURE 6. **Hind-limb clasping in a tail suspension test.** P14 mice were suspended by the tail for 25 s, and the duration of hind-limb clasping was measured. *A* and *B*, representative clasping observed in $Spr^{-/-}$ mice (*B*) but not in $Spr^{+/+}$ mice (*A*) is shown. *C*, summary of total duration of hind-limb clasping during a 25-s trial in $Spr^{+/+}$ ($n = 12$), $Spr^{+/-}$ ($n = 13$), and $Spr^{-/-}$ ($n = 14$) mice is shown. Values indicate the mean ± S.E. ***, $p < 0.001$, Kruskal-Wallis nonparametric one-way ANOVA followed by Steel-Dwass test. *Stars over bars* indicate differences between $Spr^{-/-}$ mice and wild-type mice.

showed hind-limb clasping, whereas almost none of the wild-type mice showed hind-limb clasping (Fig. 6, *A* and *B*). To quantify the clasping behavior of $Spr^{-/-}$ mice, we calculated the total duration of clasping during 25 s. As shown in Fig. 6*C*, $Spr^{-/-}$ mice showed longer clasping duration than wild-type mice.

Because hind-limb clasping was also observed in *DPS-Pts*$^{-/-}$ mice, we reanalyzed the duration of clasping posture in *DPS-Pts*$^{-/-}$ mice from previous study (16) and compared with that in $Spr^{-/-}$ mice. The duration of the clasping posture for the *DPS-Pts*$^{-/-}$ mice was 19.66 ± 0.09 s during 25 s, which was significantly longer than the duration for the $Spr^{-/-}$ mice shown in Fig. 6*C* (9.49 ± 0.15 s in $Spr^{-/-}$ mice; $p < 0.05$).

DISCUSSION

Partial biopterin deficiency leads to behavioral and psychiatric dysfunctions; however, the effect of partial biopterin deficiency on development of monoaminergic neurons has not been well characterized. In this report we examined alterations in dopamine, serotonin, and TH protein levels during the postnatal developmental period in wild-type mice and two mouse models of partial biopterin deficiency. Our results showed that dopamine and TH protein contents were markedly and concurrently increased from neonate to P21 in wild-type mice, and this increase was disturbed in the biopterin-deficient mice. Moreover, $Spr^{-/-}$ mice showed hind-limb clasping, a movement disorder, when striatal TH protein level was clearly decreased compared with wild-type mice. In addition, serotonin content in the brain was suppressed to low levels in $Spr^{-/-}$ mice. These data suggest that biopterin deficiency critically limits the normal development of both dopamine content and TH protein levels in the brain, leading to psychomotor deficits.

Taken together with our previous reports, our data suggest that the BH4 level required for normal development increases with animal growth. In neonatal animals, severe BH4 deficiency (~6% of wild-type, in the brain) leads to lethality with dramatic decreases in dopamine and TH protein levels as seen in *Pts*$^{-/-}$ mice (4). Meanwhile, moderate BH4 deficiency seen in *DPS-Pts*$^{-/-}$ mice (~36%) and $Spr^{-/-}$ mice (~26%) does not cause neonatal lethality but disturbs the augmentation of both TH protein level and dopamine content in the brain (Figs. 1 and 2). These data indicate that BH4 deficiency dose-dependently affects development of the dopaminergic system from the neonatal to early postnatal period.

Reduction of the TH protein was more prominent in nerve terminals than soma (4) and in the brain than the adrenal gland (5) in biopterin-deficient mice. Although the reason for the greater vulnerability of TH in nerve terminals by biopterin deficiency is unknown, the local concentration of biopterin may be relevant. The biopterin concentration in the brain showed a decreasing trend during the developmental period despite the elevation in the dopamine content in wild-type mice (Figs. 1 and 2). Kapatos *et al.* (18) reported a similar re-

sult for biopterin content in the brain from P0 to P50, whereas they showed a transient decline at P5. It is likely that biopterin is depleted at the nerve terminals and dendrites during the developmental period because these processes grow quickly during development. We suppose that more biopterin would be required for extending axons and dendrites during a developmental period.

The reason why TH protein levels are strongly affected by biopterin deficiency is yet to be determined. One possibility is that dopamine is required for the increase in TH protein levels because TH and dopamine form a stable and inactive complex (19, 20). Alternatively, BH4 may directly affect the stability of the TH protein (21). A recent *in vitro* study suggested that BH4 has chaperone-like activity for TH (22). Further investigation will be required to understand the regulation of TH protein levels by BH4 and dopamine *in vivo*.

In contrast to the marked increase in TH protein levels in wild-type mice, AADC protein levels were almost constant from P0 to P14 (Fig. 3*C*), which then increased in the striatum at P14 and P21, as determined immunohistochemically (Fig. 4*B*). AADC is expressed not only in catecholaminergic and serotonergic neurons but also in non-monoaminergic neurons, called D-neurons (23). The broader distribution of AADC than TH in the brain may explain the constant level of the protein during the developmental period we examined.

Phenylalanine metabolism in fetuses depends on the maternal body but becomes independent after birth (24). Consistently, phenylalanine content in *DPS-Pts*$^{-/-}$ and *Spr*$^{-/-}$ mice were relatively low at P0 and increased significantly at P7 and P14 (supplemental Fig. 1). Hyperphenylalaninemia can affect monoamine content in the brain due to a reduced supply of tyrosine and tryptophan to the brain and due to competitive inhibition of TH and tryptophan hydroxylase by a high concentration of phenylalanine (25, 26). Pascucci *et al.* (27) reported that *Pah*^{enu2} mice, which have a defect in the PAH gene, showed severe hyperphenylalaninemia and lower tyrosine content from P3 to P35, similar to *DPS-Pts*$^{-/-}$ and *Spr*$^{-/-}$ mice. However, in *Pah*^{enu2} mice, serotonin was decreased by less than 50% as compared with control mice, and dopamine levels were comparable with those of control mice at most of the postnatal days examined (27). These mild effects are in great contrast to *DPS-Pts*$^{-/-}$ and *Spr*$^{-/-}$ mice, suggesting the reduction of the monoamine content observed in *DPS-Pts*$^{-/-}$ and *Spr*$^{-/-}$ mice was mainly caused by biopterin deficiency in the brain, although the possible effect of hyperphenylalaninemia should not be excluded.

In contrast to TH protein, we found that PAH protein levels in the liver were only slightly reduced in *Spr*$^{-/-}$ mice without significant difference from wild-type mice (Fig. 5*C*). Several reports suggested that BH4 stabilizes the PAH protein (28, 29). In the liver of neonatal *Pts*$^{-/-}$ mice, PAH protein was decreased to less than 20% that in wild-type mice (29). We found that PAH protein increased with age in wild-type mice and in *Spr*$^{-/-}$ mice. This result indicates that postnatal argumentation of PAH protein was not severely perturbed by biopterin deficiency.

By immunohistochemical study, we found that striosome TH protein level in *Spr*$^{-/-}$ mice showed augmentation similar to that in wild-type mice up to P7, then the striosome TH protein level decreased thereafter, although BH4 content remained constant. These results strongly suggest that the developmental augmentation of striatal TH protein level requires increasing levels of BH4, and moderate BH4 deficiency disturbs the development of nigrostriatal dopaminergic system on the way.

Spr$^{-/-}$ mice showed hind-limb clasping at P14 (Fig. 6) when striatal TH protein level was clearly reduced. These data are in good agreement with the view that dystonia caused by BH4 deficiency is primarily mediated by dysfunction of the nigrostriatal dopaminergic projection. Interestingly, it has been reported that hind-limb clasping could be related to differential TH loss between striosome and matrix, as the TH immunoreactivity in striosomes was more greatly lost than in the surrounding matrix in *DPS-Pts*$^{-/-}$ mice (16). We did not observe such a clear difference in *Spr*$^{-/-}$ mice, although we do not know the actual alteration of activities in striosome and matrix in *Spr*$^{-/-}$ mice. The duration of the clasping posture was shorter in *Spr*$^{-/-}$ than *DPS-Pts*$^{-/-}$ mice. The reduced hind-limb clasping in *Spr*$^{-/-}$ mice may reflect the difference in the pattern of TH protein reduction in the striatum and/or noradrenergic level, which was more affected in *Spr*$^{-/-}$ mice (5).

Dopaminergic dysfunction during postnatal development results in behavioral and psychiatric abnormalities, as implicated in several neurological disorders such as attention-deficit hyperactive disorder (30). In this report we demonstrated the critical importance of biopterin content in the early postnatal period for dopamine synthesis and motor control. Our data raise the possibility that biopterin is not only essential for postnatal up-regulation of dopamine biosynthesis but also for the development and maturation of the dopaminergic system. Further investigation using *Spr*$^{-/-}$ mice and *DPS-Pts*$^{-/-}$ mice will clarify more detailed mechanisms of involuntary movements caused by biopterin deficiency.

Acknowledgments—We thank Dr. Masahiko Takada, Dr. Ryuji Kaji, and Dr. Satoshi Goto for helpful discussions and Michiko Imanishi for technical advice.

REFERENCES

1. Thöny, B., Auerbach, G., and Blau, N. (2000) *Biochem. J.* **347,** 1–16
2. Thöny, B., and Blau, N. (2006) *Hum. Mutat.* **27,** 870–878
3. Elzaouk, L., Leimbacher, W., Turri, M., Ledermann, B., Burki, K., Blau, N., and Thony, B. (2003) *J. Biol. Chem.* **278,** 28303–28311
4. Sumi-Ichinose, C., Urano, F., Kuroda, R., Ohye, T., Kojima, M., Tazawa, M., Shiraishi, H., Hagino, Y., Nagatsu, T., Nomura, T., and Ichinose, H. (2001) *J. Biol. Chem.* **276,** 41150–41160
5. Takazawa, C., Fujimoto, K., Homma, D., Sumi-Ichinose, C., Nomura, T., Ichinose, H., and Katoh, S. (2008) *Biochem. Biophys. Res. Commun.* **367,** 787–792
6. Yang, S., Lee, Y. J., Kim, J. M., Park, S., Peris, J., Laipis, P., Park, Y. S., Chung, J. H., and Oh, S. P. (2006) *Am. J. Hum. Genet.* **78,** 575–587
7. Iino, T., Tabata, M., Takikawa, S., Sawada, H., Shintaku, H., Ishikura, S., and Hara, A. (2003) *Arch. Biochem. Biophys.* **416,** 180–187
8. Park, Y. S., Heizmann, C. W., Wermuth, B., Levine, R. A., Steinerstauch, P., Guzman, J., and Blau, N. (1991) *Biochem. Biophys. Res. Commun.* **175,** 738–744
9. Ichinose, H., Ohye, T., Takahashi, E., Seki, N., Hori, T., Segawa, M.,

Nomura, Y., Endo, K., Tanaka, H., Tsuji, S., *et al.* (1994) *Nat. Genet.* **8,** 236–242
10. Segawa, M., Nomura, Y., and Nishiyama, N. (2003) *Ann. Neurol.* **54,** S32–S45
11. Blau, N., Bonafé, L., and Thöny, B. (2001) *Mol. Genet. Metab.* **74,** 172–185
12. Furukawa, Y., Nygaard, T. G., Gütlich, M., Rajput, A. H., Pifl, C., Di-Stefano, L., Chang, L. J., Price, K., Shimadzu, M., Hornykiewicz, O., Haycock, J. W., and Kish, S. J. (1999) *Neurology* **53,** 1032–1041
13. Rajput, A. H., Gibb, W. R., Zhong, X. H., Shannak, K. S., Kish, S., Chang, L. G., and Hornykiewicz, O. (1994) *Ann. Neurol.* **35,** 396–402
14. Sumi-Ichinose, C., Urano, F., Shimomura, A., Sato, T., Ikemoto, K., Shiraishi, H., Senda, T., Ichinose, H., and Nomura, T. (2005) *J. Neurochem.* **95,** 703–714
15. Nagatsu, I., Ichinose, H., Sakai, M., Titani, K., Suzuki, M., and Nagatsu, T. (1995) *J. Neural. Transm. Gen. Sect.* **102,** 175–188
16. Sato, K., Sumi-Ichinose, C., Kaji, R., Ikemoto, K., Nomura, T., Nagatsu, I., Ichinose, H., Ito, M., Sako, W., Nagahiro, S., Graybiel, A. M., and Goto, S. (2008) *Proc. Natl. Acad. Sci. U.S.A.* **105,** 12551–12556
17. Shashidharan, P., Sandu, D., Potla, U., Armata, I. A., Walker, R. H., McNaught, K. S., Weisz, D., Sreenath, T., Brin, M. F., and Olanow, C. W. (2005) *Hum. Mol. Genet.* **14,** 125–133
18. Kapatos, G., Kaufman, S., Weller, J. L., and Klein, D. C. (1983) *Brain. Res.* **258,** 351–355
19. Fujisawa, H., and Okuno, S. (2005) *Biochem. Biophys. Res. Commun.* **338,** 271–276
20. Okuno, S., and Fujisawa, H. (1985) *J. Biol. Chem.* **260,** 2633–2635
21. Urano, F., Hayashi, N., Arisaka, F., Kurita, H., Murata, S., and Ichinose, H. (2006) *J. Biochem.* **139,** 625–635
22. Thöny, B., Calvo, A. C., Scherer, T., Svebak, R. M., Haavik, J., Blau, N., and Martinez, A. (2008) *J. Neurochem.* **106,** 672–681
23. Jaeger, C. B., Teitelman, G., Joh, T. H., Albert, V. R., Park, D. H., and Reis, D. J. (1983) *Science.* **219,** 1233–1235
24. Yeoh, G. C., Edkins, E., Mackenzie, K., Fuller, S., Mercer, J. F., and Dahl, H. H. (1988) *Differentiation.* **38,** 42–48
25. Knudsen, G. M., Hasselbalch, S., Toft, P. B., Christensen, E., Paulson, O. B., and Lou, H. (1995) *J. Inherit. Metab. Dis.* **18,** 653–664
26. Ogawa, S., and Ichinose, H. (2006) *Neurosci. Lett.* **401,** 261–265
27. Pascucci, T., Andolina, D., Ventura, R., Puglisi-Allegra, S., and Cabib, S. (2008) *Brain. Res.* **1217,** 232–238
28. Pérez, B., Desviat, L. R., Gómez-Puertas, P., Martínez, A., Stevens, R. C., and Ugarte, M. (2005) *Mol. Genet. Metab.* **86,** S11–S16
29. Thöny, B., Ding, Z., and Martínez, A. (2004) *FEBS Lett.* **577,** 507–511
30. Oades, R. D. (2002) *Behav. Brain. Res.* **130,** 97–102

RESEARCH ARTICLE

Cortically Evoked Responses of Human Pallidal Neurons Recorded During Stereotactic Neurosurgery

Hiroki Nishibayashi, MD,[1]* Mitsuhiro Ogura, MD, PhD,[1] Koji Kakishita, MD, PhD,[1] Satoshi Tanaka, MD,[1] Yoshihisa Tachibana, DDS, PhD,[2] Atsushi Nambu, MD, PhD,[2] Hitoshi Kita, PhD,[3] Toru Itakura, MD, PhD[1]

[1]*Department of Neurological Surgery, Wakayama Medical University, Wakayama, Japan*
[2]*Division of System Neurophysiology, National Institute for Physiological Sciences and Department of Physiological Sciences, The Graduate University for Advanced Studies, Okazaki, Japan*
[3]*Department of Anatomy and Neurobiology, College of Medicine, University of Tennessee Memphis, Memphis, USA*

ABSTRACT: Responses of neurons in the globus pallidus (GP) to cortical stimulation were recorded for the first time in humans. We performed microelectrode recordings of GP neurons in 10 Parkinson's disease (PD) patients and 1 cervical dystonia (CD) patient during surgeries to implant bilateral deep brain stimulation electrodes in the GP. To identify the motor territories in the external (GPe) and internal (GPi) segments of the GP, unitary responses evoked by stimulation of the primary motor cortex were observed by constructing peristimulus time histograms. Neurons in the motor territories of the GPe and GPi responded to cortical stimulation. Response patterns observed in the PD patients were combinations of an early excitation, an inhibition, and a late excitation. In addition, in the CD patient, a long-lasting inhibition was prominent, suggesting increased activity along the cortico-striato-GPe/GPi pathways. The firing rates of GPe and GPi neurons in the CD patient were lower than those in the PD patients. Many GPe and GPi neurons of the PD and CD patients showed burst or oscillatory burst activity. Effective cathodal contacts tended to be located close to the responding neurons. Such unitary responses induced by cortical stimulation may be of use to target motor territories of the GP for stereotactic functional neurosurgery. Future findings utilizing this method may give us new insights into understanding the pathophysiology of movement disorders. © 2011 Movement Disorder Society

Key Words: globus pallidus; microelectrode recording; cortical stimulation; stereotactic functional neurosurgery; Parkinson's disease; dystonia

Introduction

Deep brain stimulation (DBS) is a well-established treatment for advanced movement disorders, such as Parkinson's disease (PD).[1,2] Major targets of DBS are the globus pallidus (GP) and the subthalamic nucleus (STN). Although there is a trend toward targeting more at the STN, GP-DBS has several advantages, including amelioration of drug-induced dyskinesia and fewer adverse neuropsychological effects.[3] GP-DBS is also efficient to treat severe generalized or segmental dystonia.[4] The optimal target of GP-DBS is the posteroventral part of the internal segment of the GP (GPi), corresponding to its motor territory.[3,5–7] To identify the motor territory of the GPi, microelectrode recordings (MERs) of neuronal activity, such as spontaneous firing patterns and responses to passive and active movements, have been performed.[4,8,9]

Studies in nonhuman primates have shown that stimulation of the motor cortices can identify somatotopically organized motor territories in the external segment of the GP (GPe) and GPi.[10–13] In this study, we tested whether a similar method can be used to identify motor territories in the human GP. We recorded responses of GP neurons induced by motor cortical stimulation during stereotactic neurosurgery of PD and cervical dystonia (CD) patients and

Additional Supporting Information may be found in the online version of this article.

* **Correspondence to:** Hiroki Nishibayashi, Department of Neurological Surgery, Wakayama Medical University, 811-1 Kimiidera, Wakayama, 641-0012, Japan; hirokin@wakayama-med.ac.jp

Relevant conflict of interest/financial disclosures: This study was supported by Wakayama Foundation for the Promotion of Medicine to T.I., Grants-in-Aid for Scientific Research (B) (18300135) from the Ministry of Education, Culture, Sports, Science and Technology of Japan and the Uehara Memorial Foundation to A.N., and NIH grants NS-47085 and NS-57236 to H. K. All other authors have nothing to report. Full financial disclosures and author roles can be found in the online version of this article.

Received: 26 April 2010; **Revised:** 1 September 2010; **Accepted:** 3 October 2010
Published online in Wiley Online Library (wileyonlinelibrary.com).
DOI: 10.1002/mds.23502

compared them with responses of nonhuman primates. These data will also provide clues to understanding the pathophysiology of movement disorders.

Patients and Methods

Patients

This study was approved by the ethical committee of Wakayama Medical University and has followed its guidelines. The operations were performed on 10 PD patients and 1 CD patient (Supporting Information Table 1). The 8 male and 2 female PD patients were of mean age 61.9 years (range 50–72), had a mean disease duration of 126 months (48–168), and a mean levodopa dosage of 460 mg/day (300–800). Preoperative unified Parkinson's disease rating scale (UPDRS) was a mean best score of 25.3 (0–53) and a mean worst score of 66.6 (41–93). The 62-years-old female CD patient had a disease duration of 32 months and a Toronto western spasmodic torticollis rating scale (TWSTRS) score of 54. All patients received bilateral GP-DBS electrode implantation.

Surgical Procedure and MERs

Medications were withdrawn 18 hours before operation in most patients (Supporting Information Table 1). Surgery including MERs was performed without general anesthesia in most cases. Propofol was injected intravenously (2 mL/kg/hr) if necessary (patients 2, 5, and 11). Burr holes were made bilaterally on the coronal suture about 30 mm lateral from the midline. After dural incision, a strip electrode with four platinum discs (diameter of 5 mm) spaced 10 mm apart (UZN C1-04-04-10-1-A, Unique Medical; Tokyo, Japan) was inserted into the subdural space in the posterolateral direction and placed on the upper limb area of the primary motor cortex (MI). To avoid injury to the cortical veins, special care was taken during insertion of the strip electrode and no complications were noted. Electrical stimuli (1–20 mA strength, 1.0 ms duration monophasic constant current pulse at 1 Hz) were delivered through two of the four discs. A pair of discs inducing muscle twitches in the contralateral upper limb at the lowest intensity was selected and the motor threshold (T) was determined. In the following recordings, stimuli were delivered through this pair at the intensity inducing clear muscle twitches ($1.2–1.5 \times T$) at 1 Hz. A microelectrode (FC1002, Medtronic; Minneapolis, MN) was inserted through the same burr hole targeting the tentative target in the posteroventral GPi (20 mm lateral to the midline, 4 mm ventral to the intercommissural line, and 3 mm anterior to the midcommissural point), which was determined based on the magnetic resonance imaging (MRI). Neuronal activity was amplified, displayed (Leadpoint 9033A0315, Medtronic), and fed to a computer for on-line analysis. The responses induced by MI-stimulation were assessed by constructing peristimulus time histograms (PSTHs; bin width of 1 ms) for 20–120 stimulus trials using the software (LabVIEW 7.1, National Instruments; Austin, TX). Neuronal activity was also stored on a digital audio tape (DAT) recorder (PC204Ax, SONY; Tokyo, Japan) for off-line analysis. Somatosensory responses to joint manipulations and muscle palpations of the upper limb, lower limb, and orofacial regions were also examined. We performed only one or two recording electrode penetrations in each hemisphere because this was a trial study. The GPe/GPi border (the medial medullary lamina) and the ventral border of the GPi were identified by absence of unitary activity. Based on the MERs mappings, DBS electrodes (Model 3387, Medtronic) were implanted bilaterally into the same track of MERs. The deepest electrode contact was positioned within the GPi close to the ventral border. Pulse generators were later implanted bilaterally in the chest. Monopolar (the pulse generator was used as an anode) or bipolar stimulation was applied, and the most effective contacts of DBS electrodes to improve clinical symptoms were determined. Postoperative MRI verified the position of DBS electrodes in the posteroventral GPi, and the recording sites were estimated.

Off-line Data Analysis

Neuronal activity was played back from DAT, isolated by a window discriminator, converted into digital data, and fed to a computer. Responses induced by MI-stimulation were assessed by constructing PSTHs. The mean values and standard deviations of the firing rate during 100 ms preceding the stimulation onset were calculated from PSTHs and were considered to be the values for base discharge. Responses to MI-stimulation were judged to be significant if the firing rate during at least two consecutive bins (2 ms) reached the statistical level of $P < 0.05$ (one-tailed t-test). The latency of the response was defined as the time at which the firing rate first exceeded this level. Mean firing rates and patterns were analyzed from autocorrelograms (bin width, 0.5 ms) constructed from 50 s of digitized recordings. Spontaneous firing pattern was assessed by visual inspection of the autocorrelograms: Burst activity was inferred from the existence of a single peak, and oscillatory burst activity was inferred from multiple peaks and troughs.

Results

Neuronal activity was recorded at 163 sites along 27 electrode tracks in 21 hemispheres of 11 patients (Supporting Information Table 1). Single unit activity was isolated at 157 sites, and activity of 147 neurons (59 GPe and 88 GPi) was recorded long enough to

TABLE 1. Response patterns of GPe and GPi neurons evoked by cortical stimulation and numbers of oscillatory burst neurons recorded from the PD and CD patients

	GPe			GPi		
	Cortical stimulation			Cortical stimulation		
Patient	No. of responsive neurons/no. of neurons recorded	Response patterns and no. of neurons	No. of oscillatory burst neurons	No. of responsive neurons/no. of neurons recorded	Response patterns and no. of neurons	No. of oscillatory burst neurons
PD						
1	0/0		0	0/2		1
2	1/6	1 inh	2	2/6, (5/5)	2 inh, (1 inh+ex, 4 inh)	0, (2)
3	0/1		0	0/4		0
4	4/7	1 inh, 3 late ex	0	0/12		0
5	0/0, (0/2)		0	0/0		0
6	1/2	1 inh	1	1/4	1 ex+inh+ex	2
7	0/2		0	0/5		1
8	2/2	1 ex+inh+ex, 1 inh+ex	0	2/4	1 ex+inh, 1 late ex	3
9	4/10	4 inh	1	7/17	1 ex+inh, 1 inh+ex, 1 early ex, 1 inh, 3 late ex	0
10	6/15	1 ex+inh+ex, 3 inh+ex, 1 early ex, 1 inh	1	9/14	2 ex+inh+ex, 1 ex+inh, 2 inh+ex, 3 inh, 1 late ex	2
PD total	18/45, (0/2)	2 ex+inh+ex, 4 inh+ex, 1 early ex, 8 inh, 3 late ex	5	21/68, (5/5)	3 ex+inh+ex, 3 ex+inh, 3 inh+ex, 1 early ex, 6 inh, 5 late ex, (1 inh+ex, 4 inh)	9, (2)
CD						
11	4/11, (0/1)	1 ex+inh, 1 inh+ex, 1 inh, 1 late ex	6	6/13, (1/2)	2 ex+inh, 4 inh, (1 late ex)	1, (2)
Total	22/56, (0/3)		11	27/81, (6/7)		10, (4)

Numbers in parentheses, recorded under propofol
CD, cervical dystonia; ex, excitation; GPe and GPi external and internal segments of the globus pallidus; inh, inhibition; PD, Parkinson's disease.

construct PSTHs from at least 20 stimulus trials (mean of 43) (Table 1). Among them, 137 neurons (56 GPe and 81 GPi) were recorded without general anesthesia and used for further studies. The upper limb area of the MI was successfully identified in all hemispheres tested, and the stimulus intensity of 4–16 mA was used (Supporting Information Table 1).

Responses Evoked by MI-Stimulation

Among 137 neurons, MI-stimulation induced responses in 49 neurons (36%; 22/56 in GPe, 27/81 in GPi) (Table 1). In the PD patients, response patterns to MI-stimulation were combinations of an early excitation, an inhibition, and a late excitation (Fig. 1, A1–A4). A monophasic inhibition (Fig. 1, A1) was the major response pattern (36%; 8/18 in GPe, 6/21 in GPi). Other response patterns were also observed (Table 1): a biphasic response consisting of an inhibition and a subsequent excitation (Fig. 1, A2; 18%) or an excitation and a subsequent inhibition (8%); a triphasic response consisting of an early excitation, an inhibition and a late excitation (Fig. 1, A3 and A4; 13%); and a monophasic early (5%) or late (20%) excitation. On the other hand, in the CD patient, a long-lasting monophasic inhibition (Fig. 1, A5; 50%) and a long-lasting inhibition preceded by an excitation (Fig. 1, A6; 30%) were the typical response patterns (Table 1).

The latency and duration of each component are compared in Table 2. The durations of the inhibitions in the GPe and GPi of the CD patient were significantly longer than those of the PD patients, respectively (t-test, $P < 0.05$). The latency of the inhibition in the GPi of the CD patient was significantly longer than that of the PD patients (t-test, $P < 0.01$).

Spontaneous Activity

Among 137 neurons, spontaneous activity of 71 neurons (28 GPe and 43 GPi) was recorded long enough for analysis. The mean firing rates of GPe and GPi neurons in the PD patients were significantly higher than those of GPe and GPi neurons in the CD patient, respectively (Table 2; t-test, $P < 0.05$). Besides 71 neurons, activity of six neurons was recorded under propofol administration and had a tendency to decreased activity.

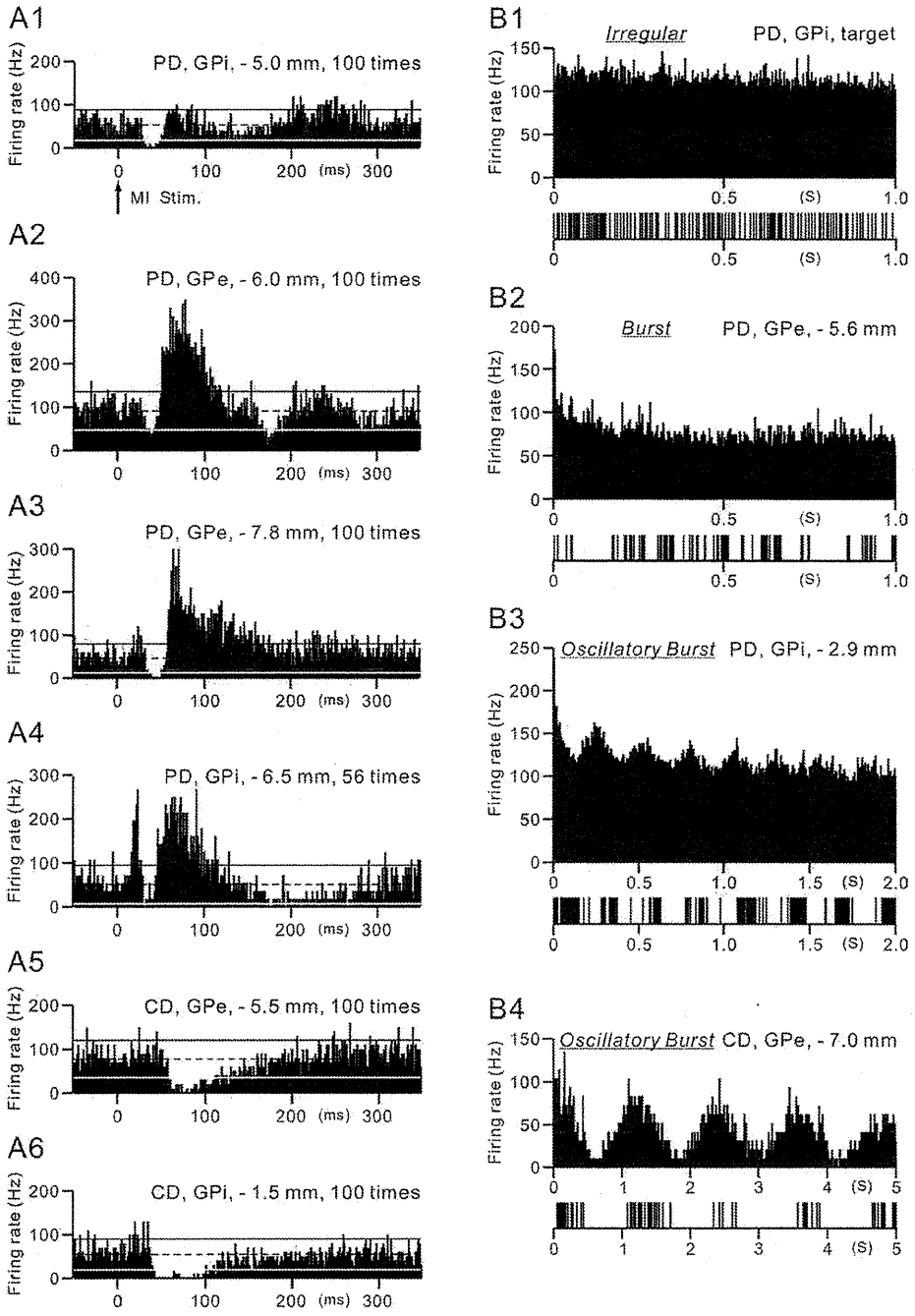

FIG. 1. A: Peristimulus time histograms (PSTHs; bin width of 1 ms) showing the responses of neurons in the external (GPe) and internal (GPi) segments of the globus pallidus evoked by stimulation of the upper limb area of the primary motor cortex in the Parkinson's disease (PD) (A1–A4) and cervical dystonia (CD) (A5 and A6) patients. Cortical stimulation was given at time = 0 (arrow in A1). Recorded sites indicated by the distance from the tentative target (negative distance, above the target) and the numbers of stimulus trials were also shown. The mean firing rate and the statistical levels of $P < 0.05$ (one-tailed t-test) calculated from the firing rate during 100 ms preceding the onset of stimulation are indicated by black dotted lines (mean), a black solid line (upper limit of $P < 0.05$), and a white solid line (lower limit of $P < 0.05$), respectively. **B**: Autocorrelograms and slow traces of digitized spikes of GPe and GPi neurons recorded from the PD (B1–B3) and CD (B4) patients. Neuronal activity can be classified into irregular, burst, and oscillatory burst types.

Based on the slow traces of digitized spikes and autocorrelograms, spontaneous firing patterns could be classified into three types: irregular, burst, and oscillatory burst (Fig. 1, B). Irregular neurons fired randomly and were characterized by the flat autocorrelogram (Fig. 1, B1). Burst neurons showed grouped discharges and a single peak around time 0 in the autocorrelogram (Fig. 1, B2). Oscillatory burst neurons showed repetitive grouped discharges and multiple cycles of peaks and troughs in the

TABLE 2. Latencies and durations of cortically evoked responses and spontaneous firing rates in GPe and GPi neurons of the PD and CD patients

	PD		CD	
	GPe	GPi	GPe	GPi
Latency (mean ± SD, ms)				
Early excitation	22.3 ± 5.0 ($n = 3$)	22.5 ± 8.8 ($n = 7$)	22.0 ($n = 1$)	22.0 ± 4.2 ($n = 2$)
Inhibition	32.6 ± 11.1($n = 14$)	34.2 ± 9.9[a] ($n = 15$)	46.0 ± 4.6 ($n = 3$)	48.7 ± 7.9[a] ($n = 6$)
Late excitation	60.7 ± 14.4 ($n = 9$)	56.2 ± 14.3 ($n = 11$)	79.0 ± 31.1($n = 2$)	(-)
Duration (mean ± SD, ms)				
Early excitation	6.3 ± 7.5 ($n = 3$)	5.8 ± 4.4 ($n = 7$)	16.0 ($n = 1$)	2.5 ± 0.71 ($n = 2$)
Inhibition	16.1 ± 7.4[b] ($n = 14$)	19.1 ± 12.2[c] ($n = 15$)	42.3 ± 34.6[b] ($n = 3$)	37.5 ± 15.6[c] ($n = 6$)
Late excitation	27.6 ± 33.7 ($n = 9$)	25.7 ± 39.2 ($n = 11$)	2.5 ± 0.71 ($n = 2$)	(-)
Spontaneous firing rate	81.0 ± 52.5[d] ($n = 17$)	92.7 ± 40.1[e] ($n = 34$)	45.8 ± 17.6[d] ($n = 11$)	62.3 ± 12.1[e] ($n = 9$)
(mean ± SD, Hz)	[-]	[47.2 ± 23.6 ($n = 3$)]	[46.7 ($n = 1$)]	[27.1 ± 36.7 ($n = 2$)]

Values in brackets, recorded under propofol.
[a]$P < 0.01$.
[b,c,d,e]$P < 0.05$, significantly different from each other (*t*-test).

autocorrelogram (Fig. 1, B3 and B4). Most neurons [94% (16/17) in GPe and 68% (23/34) in GPi in PD, 100% (11/11) in GPe and 78% (7/9) in GPi in CD] showed burst or oscillatory burst activity (Table 3). In the PD patients, more GPe neurons showed burst or oscillatory burst activity than GPi neurons ($P < 0.05$, Fisher's exact test). Oscillatory frequency of oscillatory burst neurons in the PD patients was mostly in the delta (1–4 Hz) or theta–alpha (4–12 Hz) band, while that in the CD patient was mostly in the delta band.

Locations of Recorded Neurons

Locations of recorded neurons are plotted in Figure 2. GPe/GPi neurons responding to MI-stimulation were found in clusters along electrode tracks, although the rostral and the lateral part of the GPe were not explored. Among 49 GPe/GPi neurons responding to MI-stimulation, 12 neurons (24%) responded to passive movements of the upper limb, such as shoulder, elbow, wrist, or digits. On the other hand, among 43 GPe/GPi neurons responding to passive movements of the upper limb, 12 neurons (28%) responded to MI-stimulation. Neurons responding to passive movements of the lower limb were found in the different area from the upper limb area. Neurons responding to jaw movements were mainly found in the ventral to middle part of the GPi.

Correlation between Clinical Benefits and Neuronal Responses

Monopolar (14 sides) or bipolar (eight sides) electrical stimulation (1.5–3.5 V constant voltage, 210 μs duration, at 185 Hz) was applied for DBS. The most effective cathodal contacts were located in the dorsal (11 sites), middle (two sites), ventral (six sites) GPi, or ventral GPe (three sites; Fig. 2, Supporting Information Table 2). For the PD patients, symptoms were assessed using UPDRS III and IV (items 18–35) before and 10–20 days after starting DBS (Supporting Information Table 2). Symptoms were ameliorated in all patients, and the DBS was markedly effective (score ≥ 10) in four patients (patients 2, 6, 8, and 10) and fairly effective (score ≥ 5) in other four patients (patients 3, 4, 7, and 9). Noticeably improved symptoms (score ≥ 4) were rigidity (patients 2, 3, 7, 8, and 10), bradykinesia (patients 2, 6, 8, and 10), tremor (patients 4, 6, and 8), and dyskinesia (patient 10). In the CD patient, the TWSTRS score decreased from 54 to 34, and unilateral cervical rotation was markedly improved. The most effective cathodal contacts tended to be located close to the responding neurons (Fig. 2).

Discussion

Responses Evoked by MI-Stimulation

In this study, the responses of GPe/GPi neurons induced by MI-stimulation were composed of various combinations of an early excitation, an inhibition, and a late excitation in human subjects. In the GPe, GPi and substantia nigra pars reticulata (SNr) of monkeys

TABLE 3. Spontaneous firing patterns of GPe and GPi neurons recorded from the PD and CD patients

	PD		CD	
Spontaneous firing pattern	GPe	GPi	GPe	GPi
Irregular	1	11	0	2
Burst	11	14	5	6
Oscillatory burst	5	9	6	1
<4 Hz	3	3	6	1
4–12 Hz	2	5	0	0
12 Hz<	0	1	0	0
Total	17	34	11	9

Numbers of GPe and GPi neurons exhibiting irregular, burst, or oscillatory burst activity are shown.

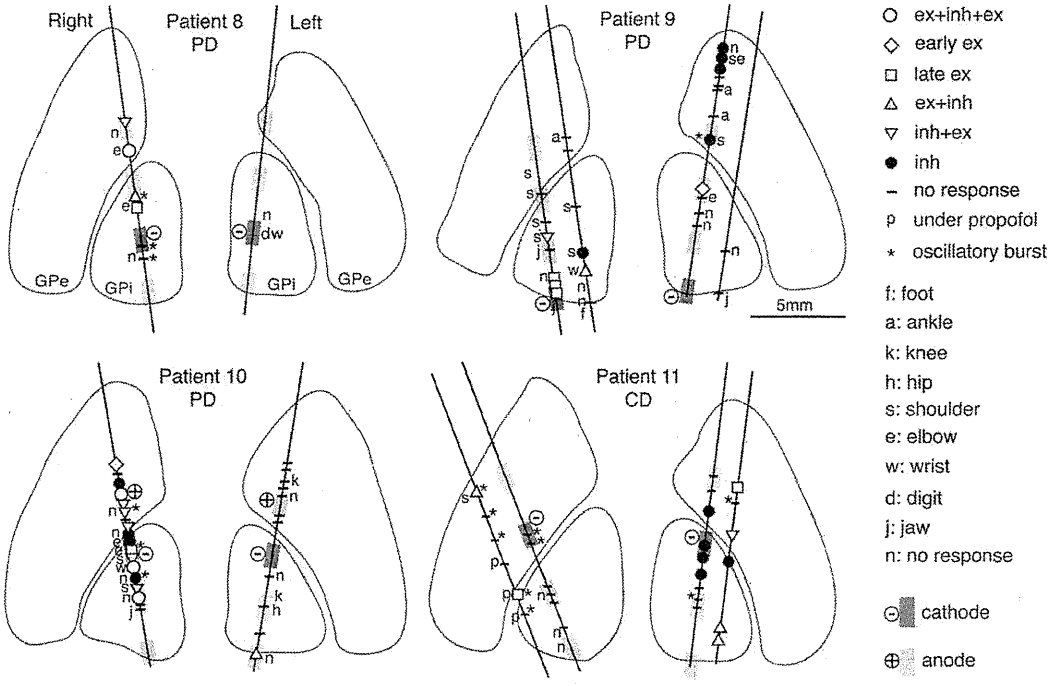

FIG. 2. Locations of recorded neurons in the GPe and GPi of the PD (patients 8, 9, and 10) and CD (patient 11) patients shown in coronal views. Response patterns evoked by cortical stimulation and somatosensory inputs examined by passive manipulations were represented by different symbols. Locations of DBS electrodes were also shown by shaded rectangles (dark rectangle with minus sign, the most effective cathode; light rectangle with plus sign, anode used). In patients 8, 9, and 11, monopolar stimulation was performed using the pulse generator as an anode.

and rodents, cortical stimulation evoked typically a triphasic response, composed of an early excitation, an inhibition, and a late excitation,[10–16] which is very similar to the triphasic response observed in this study (Fig. 1, A3 and A4). Studies in nonhuman primates have clarified that the early excitation is derived from the cortico-STN-GPe/GPi pathway,[10] the inhibition by the cortico-striato-GPe/GPi pathway, and the late excitation by the cortico-striato-GPe-STN-GPe/GPi pathway.[12,13] We assume that the response components observed in the present human study were derived from the same pathways. However, a major response pattern in human patients was a monophasic inhibition. Such a pattern difference may be ascribed to the stimulus methods. Although stimulating wire electrodes were implanted inside the cortex of animals, disc electrodes on the cortical surface in this study may less effectively stimulate cortico-STN neurons, which are located in the deeper layer than corticostriatal neurons. The latencies of response components in this study (Table 2) were two times longer than those in monkeys[10–13] and three times longer than those in rodents.[14–16] These latency differences may be ascribed to the following reasons: (1) larger size of the human brain; (2) surface electrodes in this study may stimulate cortical neurons indirectly through afferent fibers or apical dendrites, whereas wire electrodes in animal studies may stimulate directly and instantly somata and axons; (3) pathological changes in PD.

Somatotopic Representations in the GPe/GPi

The somatotopic representations in the GPe/GPi have been repeatedly studied by movement-related activity during task performance, somatosensory inputs from muscles and joints, responses evoked by cortical stimulation and anatomical methods in nonhuman primates.[11,17,18] In the caudal part of the GPe/GPi, the orofacial area is represented in the most ventral part, and the lower limb area is found in the dorsal part. The upper limb area is located in between. The similar somatotopic representations were also reported in humans during stereotactic surgery.[19] The upper limb area occupies a large region in the GPe/GPi and is a good target to search during surgery. In this study, we have succeeded in identifying the upper limb area in the GPe/GPi by neuronal responses evoked by MI-stimulation, as well as by somatosensory inputs.

Targeting the Motor Territories of the GPe/GPi

The motor territory of the GPi is usually identified during stereotactic surgery by conventional electrophysiological methods, such as observing responses to passive/active movements.[8,9] The method introduced in this study, examining the unitary responses induced by MI-stimulation, can also identify the motor territories of the GPe/GPi. Some neurons that responded to MI-stimulation did not show somatosensory responses

probably because stimulus conditions were not optimal, especially during surgery. The effective cathodal contacts tended to be located close to the responding neurons. On the other hand, this method is more complex and time-consuming than the conventional ones, and thus, it is more appropriate in special cases, such as in patients under sedation, with considerable damage or with previous lesions in the basal ganglia; when spontaneous firing patterns or somatosensory responses are less obvious; and in cases aimed for research purposes.

Pathophysiology of Movement Disorders

There are many reports on GPe/GPi activity in PD patients and parkinsonian monkeys.[20–23] Decreased activity along the striato-GPi direct pathway and increased activity along the striato-GPe indirect pathway have been considered to cause increased GPi activity and finally interfere with disinhibitory process of releasing appropriate movements in PD.[24] Although not significant, firing rate of GPi neurons was higher than that of GPe neurons in this study (Table 2), supporting the firing rate theory. However, this study failed to show difference in durations of inhibitions between GPe and GPi neurons. Contrary to the firing rate theory, recent studies have focused on abnormal burst and oscillatory activity in the GPe/GPi underlying the PD pathophysiology.[25] Most neurons in this study showed burst or oscillatory burst activity.

On the other hand, reports on GPe/GPi activity in CD patients are limited.[26] The GPi firing rate in CD patients was lower than that in PD patients. GPi neurons fired in a more irregular pattern with more frequent and longer pauses in CD patients compared with PD patients. GPe/GPi activity in generalized dystonia decreased and became bursty.[27,28] The present data showed decreased GPe/GPi activity in the CD patient compared with the PD patients, and burst and oscillatory burst activity, agreeing with the previous reports.[26] Moreover, MI-stimulation induced a long-lasting inhibition in the GPe/GPi (Fig. 1, A5 and A6), suggesting increased activity along the cortico-striato-GPe/GPi pathway. Recently, the mouse model of dystonia also showed a long-lasting inhibition evoked by cortical stimulation in the GPe/GPi,[16] which is very similar to that observed in this study. Thus, increased activity along both the cortico-striato-GPi direct and cortico-striato-GPe indirect pathways is considered to be a fundamental change in dystonia. Reduced GPi output should disinhibit thalamic and cortical activity, resulting in involuntary movements observed in dystonia.

References

1. Rodriguez-Oroz MC, Obeso JA, Lang AE, et al. Bilateral deep brain stimulation in Parkinson's disease: a multicentre study with 4 years follow-up. Brain 2005;128:2240–2249.
2. Volkmann J, Allert N, Voges J, Sturm V, Schnitzler A, Freund HJ. Long-term results of bilateral pallidal stimulation in Parkinson's disease. Ann Neurol 2004;55:871–875.
3. Peppe A, Pierantozzi M, Altibrandi MG, et al. Bilateral GPi DBS is useful to reduce abnormal involuntary movements in advanced Parkinson's disease patients, but its action is related to modality and site of stimulation. Eur J Neurol 2001;8:579–586.
4. Starr PA, Turner RS, Rau G, et al. Microelectrode-guided implantation of deep brain stimulators into the globus pallidus internus for dystonia: techniques, electrode locations, and outcomes. J Neurosurg 2006;104:488–501.
5. Lombardi WJ, Gross RE, Trepanier LL, Lang AE, Lozano AM, Saint-Cyr JA. Relationship of lesion location to cognitive outcome following microelectrode-guided pallidotomy for Parkinson's disease: support for the existence of cognitive circuits in the human pallidum. Brain 2000;123:746–758.
6. Vitek JL, Bakay RA, Hashimoto T, et al. Microelectrode-guided pallidotomy: technical approach and its application in medically intractable Parkinson's disease. J Neurosurg 1998;88:1027–1043.
7. Yelnik J, Damier P, Bejjani BP, et al. Functional mapping of the human globus pallidus: contrasting effect of stimulation in the internal and external pallidum in Parkinson's disease. Neuroscience 2000;101:77–87.
8. Hutchison WD, Lozano AM.Microelectrode recordings in movement disorder surgery. In: Lozano AM, editor. Movement disorder surgery. Basel: Karger; 2000. p 103–117. (Progress in Neurological Surgery; Vol. 15).
9. Kaplitt MG, Hutchison WD, Lozano AM.Target localization in movement disorders surgery. In: Tarsy D, Vitek JL, Lozano AM, editors. Surgical treatment of Parkinson's disease and other movement disorders. Totowa: Humana Press; 2003. p 87–98.
10. Nambu A, Tokuno H, Hamada I, et al. Excitatory cortical inputs to pallidal neurons via the subthalamic nucleus in the monkey. J Neurophysiol 2000;84:289–300.
11. Yoshida S, Nambu A, Jinnai K. The distribution of the globus pallidus neurons with input from various cortical areas in the monkeys. Brain Res 1993;611:170–174.
12. Kita H, Nambu A, Kaneda K, Tachibana Y, Takada M. Role of ionotropic glutamatergic and GABAergic inputs on the firing activity of neurons in the external pallidum in awake monkeys. J Neurophysiol 2004;92:3069–3084.
13. Tachibana Y, Kita H, Chiken S, Takada M, Nambu A. Motor cortical control of internal pallidal activity through glutamatergic and GABAergic inputs in awake monkeys. Eur J Neurosci 2008; 27:238–253.
14. Maurice N, Deniau JM, Glowinski J, Thierry AM. Relationships between the prefrontal cortex and the basal ganglia in the rat: physiology of the cortico-nigral circuits. J Neurosci 1999;19: 4674–4681.
15. Ryan LJ, Clark KB. The role of the subthalamic nucleus in the response of globus pallidus neurons to stimulation of the prelimbic and agranular frontal cortices in rats. Exp Brain Res 1991;86: 641–651.
16. Chiken S, Shashidharan P, Nambu A. Cortically evoked long-lasting inhibition of pallidal neurons in a transgenic mouse model of dystonia. J Neurosci 2008;28:13967–13977.
17. DeLong MR, Crutcher MD, Georgopoulos AP. Primate globus pallidus and subthalamic nucleus: functional organization. J Neurophysiol 1985;53:530–543.
18. Strick PL, Dum RP, Picard N. Macro-organization of the circuits connecting the basal ganglia with the cortical motor areas. In: Houck JC, Davis JL, Beiser DG, editors. Models of information processing in the basal ganglia. Cambridge: MIT Press; 1995. p 117–130.
19. Guridi J, Gorospe A, Ramos E, Linazasoro G, Rodriguez MC, Obeso JA. Stereotactic targeting of the globus pallidus internus in Parkinson's disease: imaging versus electrophysiological mapping. Neurosurgery 1999;45:278–287; discussion 287–279.
20. Bergman H, Wichmann T, Karmon B, DeLong MR. The primate subthalamic nucleus. II. Neuronal activity in the MPTP model of parkinsonism. J Neurophysiol 1994;72:507–520.
21. Raz A, Vaadia E, Bergman H. Firing patterns and correlations of spontaneous discharge of pallidal neurons in the normal and the tremulous 1-methyl-4-phenyl-1,2,3,6-tetrahydropyridine vervet model of parkinsonism. J Neurosci 2000;20:8559–8571.

22. Hutchison WD, Levy R, Dostrovsky JO, Lozano AM, Lang AE. Effects of apomorphine on globus pallidus neurons in parkinsonian patients. Ann Neurol 1997;42:767–775.

23. Magnin M, Morel A, Jeanmonod D. Single-unit analysis of the pallidum, thalamus and subthalamic nucleus in parkinsonian patients. Neuroscience 2000;96:549–564.

24. DeLong MR. Primate models of movement disorders of basal ganglia origin. Trends Neurosci 1990;13:281–285.

25. Brown P. Abnormal oscillatory synchronisation in the motor system leads to impaired movement. Curr Opin Neurobiol 2007;17:656–664.

26. Tang JK, Moro E, Mahant N, et al. Neuronal firing rates and patterns in the globus pallidus internus of patients with cervical dystonia differ from those with Parkinson's disease. J Neurophysiol 2007;98:720–729.

27. Vitek JL, Chockkan V, Zhang JY, et al. Neuronal activity in the basal ganglia in patients with generalized dystonia and hemiballismus. Ann Neurol 1999;46:22–35.

28. Starr PA, Rau GM, Davis V, et al. Spontaneous pallidal neuronal activity in human dystonia: comparison with Parkinson's disease and normal macaque. J Neurophysiol 2005;93:3165–3176.

EJN fens EUROPEAN JOURNAL OF NEUROSCIENCE

European Journal of Neuroscience, Vol. 33, pp. 285–297, 2011 doi:10.1111/j.1460-9568.2010.07492.x

NEUROSYSTEMS

Origins of multisynaptic projections from the basal ganglia to rostrocaudally distinct sectors of the dorsal premotor area in macaques

Yosuke Saga,[1,*] Yoshihiro Hirata,[2,3,*] Daisuke Takahara,[2,3,4,*] Ken-ichi Inoue,[2,3,*] Shigehiro Miyachi,[5] Atsushi Nambu,[4] Jun Tanji,[1] Masahiko Takada[2,3] and Eiji Hoshi[1]

[1]Tamagawa University Brain Science Institute, Machida, Tokyo, Japan
[2]Systems Neuroscience Section, Primate Research Institute, Kyoto University, Inuyama, Japan
[3]Department of System Neuroscience, Tokyo Metropolitan Institute for Neuroscience, Tokyo Metropolitan Organization for Medical Research, Tokyo, Japan
[4]Division of System Neurophysiology, National Institute for Physiological Sciences and Department of Physiological Sciences, Graduate University for Advanced Studies (SOKENDAI), Okazaki, Japan
[5]Cognitive Neuroscience Section, Primate Research Institute, Kyoto University, Inuyama, Japan

Keywords: behavioral and cognitive neuroscience, CVS-11, motor control, rabies virus, transneuronal transport

Abstract

We examined the organization of multisynaptic projections from the basal ganglia (BG) to the dorsal premotor area in macaques. After injection of the rabies virus into the rostral sector of the caudal aspect of the dorsal premotor area (F2r) and the caudal sector of the caudal aspect of the dorsal premotor area (F2c), second-order neuron labeling occurred in the internal segment of the globus pallidus (GPi) and the substantia nigra pars reticulata (SNr). Labeled GPi neurons were found in the caudoventral portion after F2c injection, and in the dorsal portion at the rostrocaudal middle level after F2r injection. In the SNr, F2c and F2r injections led to labeling in the caudal or rostral part, respectively. Subsequently, third-order neuron labeling was observed in the external segment of the globus pallidus (GPe), the subthalamic nucleus (STN), and the striatum. After F2c injection, labeled neurons were observed over a broad territory in the GPe, whereas after F2r injection, labeled neurons tended to be restricted to the rostral and dorsal portions. In the STN, F2c injection resulted in extensive labeling over the nucleus, whereas F2r injection resulted in labeling in the ventral portion only. After both F2r and F2c injections, labeled neurons in the striatum were widely observed in the striatal cell bridge region and neighboring areas, as well as in the ventral striatum. The present results revealed that the origins of multisynaptic projections to F2c and F2r in the BG are segregated in the output stations of the BG, whereas intermingling rather than segregation is evident with respect to their input station.

Introduction

The circuits connecting the basal ganglia (BG) and the cerebral cortex play central roles in a variety of brain functions, including those involving emotional, motivational, cognitive and motor aspects (Alexander *et al.*, 1986; Middleton & Strick, 2000b; Lichter & Cummings, 2001; Graybiel, 2008). Because of the critical role of the BG in both normal and disordered brain functions, understanding of the cortico-BG circuits is crucial. Recently, tract-tracing studies with trans-synaptic transport of a neurotropic virus have revealed that different portions of the internal segment of the globus pallidus (GPi) and the substantia nigra pars reticulata (SNr) send outputs to distinct cortical areas via the thalamus, suggesting that the BG possesses multiple parallel output channels (Alexander & Crutcher, 1990; Hoover & Strick, 1993; Middleton & Strick, 1996a; Hoover & Strick, 1999; Middleton & Strick, 2000a, 2002; Clower *et al.*, 2005; Draganski *et al.*, 2008). On the other hand, it has been reported that there is a divergence–reconvergence architecture in the outflow from the cerebral cortex to the globus pallidus through the striatum (Flaherty & Graybiel, 1993a, 1994), and that distributed striatal regions receive inputs from distinct cortical areas (Künzle, 1975, 1977; Yeterian & Van Hoesen, 1978; Selemon & Goldman-Rakic, 1985; Arikuni & Kubota, 1986; Yeterian & Pandya, 1991; Flaherty & Graybiel, 1993b, 1994; Inase *et al.*, 1996; Takada *et al.*, 1998a, 2001; Inase *et al.*, 1999; Nambu *et al.*, 2002; Tachibana *et al.*, 2004).

In this study, we examined the organization of multisynaptic inputs from the BG to the caudal aspect of the dorsal premotor area (F2) in Brodmann's area six of macaques (Brodmann, 1905; Matelli *et al.*, 1985; Barbas & Pandya, 1987). Physiological studies have shown that

Correspondence: Masahiko Takada, [2]Systems Neuroscience Section, as above.
E-mail: takada@pri.kyoto-u.ac.jp
Eiji Hoshi, [1]Tamagawa University Brain Science Institute, as above.
E-mail: hoshie@lab.tamagawa.ac.jp

*Y.S., Y.H., D.T. and K.I. contributed equally to this work.

Received 4 July 2010, revised 6 September 2010, accepted 5 October 2010

F2 plays a crucial role in the planning and execution of arm movements (Wise, 1985; Caminiti *et al.*, 1998; Hoshi & Tanji, 2007; Cisek & Kalaska, 2010), and that functional specialization between the caudal sector of F2 (F2c), located ventral to the superior precentral dimple, and the rostral sector of F2 (F2r), located dorsal to the genu of the arcuate sulcus, exists (Cisek *et al.*, 2003; Hoshi & Tanji, 2006). On the basis of our previous results demonstrating that F2r and F2c receive largely segregated inputs from the cerebellum (Hashimoto *et al.*, 2010), it is of great interest to examine the origins of projections from the BG to F2c and F2r in macaques. In this study, we show that the origins of multisynaptic projections to F2c and F2r in the BG are segregated in the output stations of the BG (i.e. the GPi and SNr), whereas intermingling rather than segregation is evident with respect to the other BG components, including their input station (i.e. the striatum). Furthermore, multiple patches within the striatum project to F2 multisynaptically. These results indicate that the circuits linking the BG and F2 consist of parallel divergent channels at the output stage, and possess a common convergent window at the input stage.

Materials and methods

Animals

We used seven Japanese monkeys (*Macaca fuscata*) and one rhesus (*Macaca mulatta*) monkey weighing 4.0–7.6 kg (Table 1). These were the same animals as used in our previous study (Hashimoto *et al.*, 2010). The experimental protocol was approved by the Animal Care and Use Committee of the Tokyo Metropolitan Institute for Neuroscience, and all experiments were conducted in accordance with the Guidelines for the Care and Use of Animals (Tokyo Metropolitan Institute for Neuroscience, 2000).

Surgical procedures

General anesthesia of the monkeys was induced with ketamine hydrochloride (10 mg/kg, i.m.) and maintained with sodium pentobarbital (20 mg/kg, i.v.). During the surgical operation, hydration was maintained with lactated Ringer's solution (i.v.). An antibiotic [ceftriaxone (Rocephin); 75 mg/kg, i.m.] was administered at the time of initial anesthesia. Each monkey's head was secured in a stereotaxic frame, and the skin and muscle were retracted to expose the skull over the left hemisphere. A large craniotomy was made over the left frontal lobe, and the dura mater was cut to expose the superior limb of the arcuate sulcus, the genu of the arcuate sulcus (located approximately 20 mm anterior to the interaural line in the Horsley–Clark coordinate), the superior precentral dimple, and the central sulcus, allowing us to visually inspect the injection sites on the cortical surface. In three of the eight monkeys, we administered dexamethasone (Decadron; 0.5 mg/kg, i.m.), because they showed signs of a slight swelling of the exposed area. Soon after administration, the cortex returned to normal. After confirming this, we started the viral injections.

Viral injections

The virus was obtained from the Centers for Disease Control and Prevention (Atlanta, GA, USA) and donated by S. Inoue (The National Institute of Infectious Diseases, Tokyo, Japan). The titer of a stock viral suspension was 1.4×10^8 focus-forming units/mL. The location of each injection site was based on surface landmarks and their known relationships to the caudal sector of the dorsal premotor area (Fig. 1A) (Matelli *et al.*, 1985). Injection sites of F2c included the area dorsal to the spur of the arcuate sulcus and below the superior precentral dimple (Fig. 1B). Injection sites in F2r included an area 3 mm rostral to the genu of the arcuate sulcus in the posterior bank of the superior limb of the arcuate sulcus (Fig. 1C). The viral suspension was injected through a 10-μL Hamilton microsyringe. For each injection track, viral deposits were placed at two different depths: 4 and 2 mm below the cortical surface in F2r injections, and 2 and 1.5 mm below the cortical surface in F2c injections. At each depth, 0.5 μL of the viral suspension was deposited. When injections were complete, the dura mater and bone flap were repositioned, and the scalp incision was closed. An analgesic [buprenorphine (Buprenex); 0.01 mg/kg, i.m.] was administered after surgery.

Histology

After surviving for 3 or 4 days, the monkeys were deeply anesthetized with an overdose of sodium pentobarbital (50 mg/kg) and killed by perfusion–fixation with a mixture of 10% formalin and 15% saturated picric acid in a 0.1 M phosphate buffer (pH 7.4). The brain was removed from the skull, postfixed in the same fresh fixative overnight at 4 °C, and placed in a 0.1 M phosphate buffer (pH 7.4) containing 30% sucrose. Coronal sections with a thickness of 50 μm were cut serially on a freezing microtome. Every sixth section was processed for immunohistochemical staining for rabies virus by means of the standard avidin–biotin–peroxidase complex method. Following immersion in 1% skimmed milk, the sections were incubated overnight with rabbit anti-rabies virus antibodies in 0.1 M phosphate-buffered saline (pH 7.4) containing 0.1% Triton X-100 and 1% normal goat serum. The antibody was donated by S. Inoue (The National Institute of Infectious Diseases, Tokyo, Japan). The sections were then placed in the same fresh incubation medium containing biotinylated goat anti-rabbit IgG antibody (diluted 1 : 200; Vector Laboratories, Burlingame, CA, USA), followed by the avidin–biotin–peroxidase complex kit (ABC Elite; Vector Laboratories). To visualize the antigen, the sections were reacted in a 0.05 M Tris–HCl buffer (pH 7.6) containing 0.04% diaminobenzidine, 0.04% nickel chloride, and 0.002% hydrogen peroxide.

TABLE 1. Summary of experiments

Monkey	Species	Injection site	Survival (days)	No. of injection tracks	Injection volume (μL)
Bei	*Macaca fuscata*	F2c	3	4	4.0
Chi	*M. fuscata*	F2c	3	4	4.0
06–23	*M. fuscata*	F2r	3	3	3.0
Hyu	*Macaca mulatta*	F2r	3	3	3.0
Ams	*M. fuscata*	F2c	4	4	4.0
Del	*M. fuscata*	F2c	4	4	4.0
06–22	*M. fuscata*	F2r	4	3	3.0
Itt	*M. fuscata*	F2r	4	3	3.0

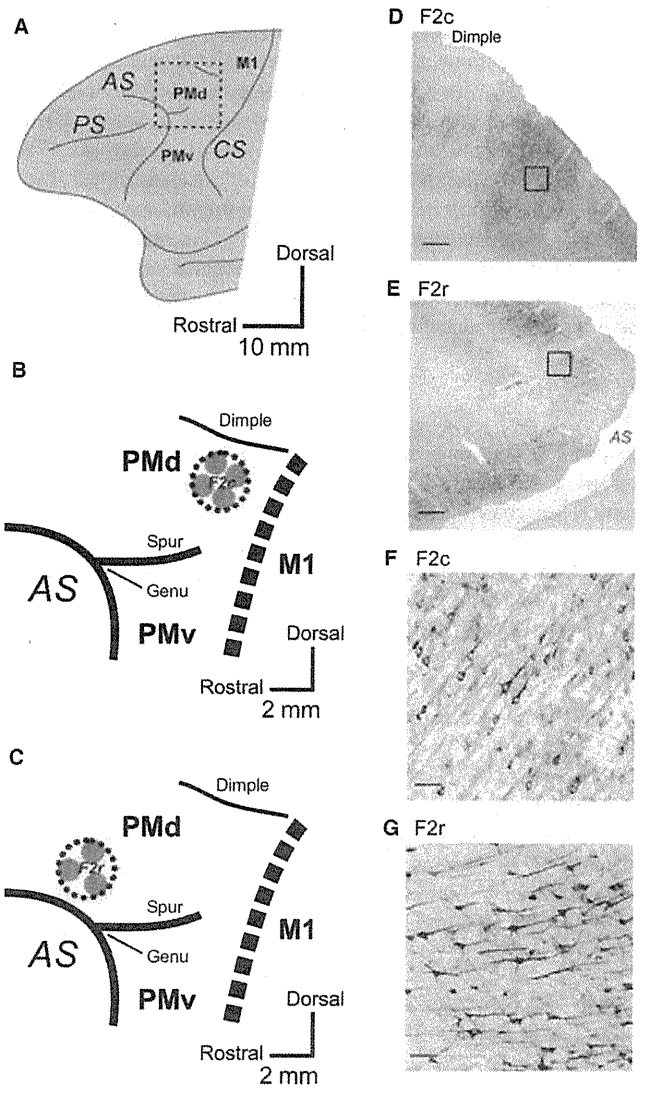

FIG. 1. Locations of the injection sites in F2r and F2c. (A) Diagram illustrating the macaque lateral frontal lobe. The rectangular area drawn with broken lines in A is enlarged in B and C. B and C are the injection sites of the rabies virus in F2c (B) and F2r (C). Within each site, small circles in gray (0.5 mm in radius) indicate the estimated viral spread around the injection tracks. In B and C, the border between the premotor areas (PMd, dorsal premotor area; PMv, ventral premotor area) and M1 is represented by the broken line. (D–G) Low-magnification and high-magnification photomicrographs of the injection sites 3 days after rabies injection. (D and F) The injection was made into F2c (monkey Chi). (E and G) The injection was made into F2r (monkey 06–23). In the low-power images (D and E), labeled neurons are densely distributed at the injection sites. In the high-power images (F and G), many neurons are seen to be labeled in a Golgi-like manner. The boxed region in D and E is enlarged in F and G. AS, arcuate sulcus; CS, central sulcus; Dimple, superior precentral dimple; Genu, genu of AS; PS, principal sulcus; Spur, spur of AS. Scale bars in D and E: 500 μm. Scale bars in F and G: 50 μm.

Safety issues

All experiments were performed in a special primate laboratory (biosafety level 2) designated for *in vivo* virus experiments. Throughout the experiments, the monkeys were kept in individual cages that were installed inside a special safety cabinet. To avoid accidental infection with the virus, all investigators received immunization before the procedures and wore protective clothing during the experimental sessions. Equipment was disinfected with 80% (v/v) ethanol after each experimental session, and waste was autoclaved prior to disposal.

Analytical procedures

We digitized the outline of the nuclei of the BG and the location of labeled neurons with the MD-Plot 3 system (Accustage, Shoreview, MN, USA) attached to a microscope system (Nikon Eclipse 80i, Tokyo, Japan). Neuronal labeling was plotted on tracings of equidistant coronal sections (separated by 300 μm) throughout the BG. To examine the distribution and density of labeled neurons in the GPi, the external segment of the globus pallidus (GPe), and the SNr, we constructed two-dimensional density maps. For this purpose, we developed a program that operates on MATLAB (Mathworks, Natick, MA, USA). This program allowed us to load and display the digitized data from each section, to place landmarks on the displayed section, and to draw a line onto which labeled neurons were projected. It further allowed us to align the positions of the labeled neurons with landmarks in multiple sections. Using this program, we drew a curved line on each coronal section midway between the medial and lateral outlines of the outer and inner portions of the GPi (Fig. 4A) and GPe (Fig. 8A), and between the dorsal and ventral outlines of the SNr (Fig. 6A). The position of each labeled neuron was projected onto the central line. Then, each line through the nucleus was aligned on the ventral edges of the GPi (Fig. 4A) and GPe (Fig. 8A) or the lateral edge of the SNr (Fig. 6A).

To construct the density map of labeled neurons in the subthalamic nucleus (STN), we counted the number of the labeled neurons within a 300 × 300-μm bin on the coronal section and displayed the results as a color-coded density map (Fig. 9). To construct the density map of labeled neurons in the striatum, we counted the number of the labeled neurons within a 500 × 500-μm bin on the coronal section and displayed the results as a color-coded density map (Fig. 10). A color code was assigned to each bin in each map of the STN and striatum to indicate the number of labeled neurons included.

Results

Multiple injections of rabies virus were made into F2r or F2c (Fig. 1; Table 1) of eight monkeys. The injection sites (Fig. 1B and C) were determined on the basis of the results of our previous electrophysiological study, in which we showed that the neuronal response properties involved in planning and executing reaching movements differed in F2r and F2c (Hoshi & Tanji, 2006). This rostrocaudal segregation is consistent with the classification scheme that emerged in previous studies (Barbas & Pandya, 1987; Matelli *et al.*, 1998; Luppino *et al.*, 2003). Multiple injections were administered at four points (approximately 1 mm apart) lateral to the superior precentral dimple during the F2c procedure (Fig. 1B). During the F2r procedure, multiple injections were administered at three points (one at the level of the genu of the arcuate sulcus and two ≤2 mm rostral to the genu; Fig. 1C). In the 3-day post-injection period, labeled neurons were densely distributed at the injection sites (Fig. 1D and E). For many labeled neurons, not only cell bodies but also dendritic trees were clearly visible (Fig. 1F and G). Because infected neurons displayed no evidence of cell lysis or tissue damage, it was rather difficult to estimate the extent of the injection sites. However, there are two studies relevant to this issue. First, in our previous study (Miyachi *et al.*, 2005), neuronal labeling seen at the injection site was examined on the second day after rabies injection, when only first-order neurons projecting directly to the injection site were labeled. We found the

labeled neurons to be restricted to a radius of < 500 μm around the injection needle track. Second, by analyzing the density of labeled neurons at different time points after rabies injection, Kelly & Strick (2003) concluded that the effective site of rabies (CVS-11) uptake was confined to an area within a radius of 500 μm for each needle penetration in the case of 0.2–1 μL of the injection. On the basis of these studies, we considered that the viral spread at the injection site would be estimated at < 500 μm in radius around the needle track, and that the actual size of the rabies injection was comparable in the F2r and F2c injection cases.

Origins of projections to F2c and F2r from the output nuclei of the BG (GPi and SNr)

Three days after the rabies injection into F2c or F2r, a number of labeled neurons were observed in the GPi and SNr (Fig. 2A, B, D, and E). These neurons were deemed to send output to F2c or F2r via the ventral nuclei or mediodorsal nucleus of the thalamus. No labeled neurons were found in the GPe at this stage, indicating that only second-order neuron labeling occurred in the 3-day post-injection period.

GPi

The distribution of labeled neurons observed in the GPi after the F2c injection differed from that observed after the F2r injection (Fig. 3). Two-dimensional density maps of the GPi were prepared to separately represent the labeling patterns in the outer and inner portions (Fig. 4A). These maps show that the distributions of GPi neurons projecting to F2c and F2r were segregated in both portions, each of which received input from the striatum (Kaneda *et al.*, 2002). After F2c injection, labeled neurons were distributed broadly in the ventral part of the GPi at its caudal level (Fig. 4B and C). By contrast, labeled neurons after F2r injection were located in the dorsal part of the GPi at its rostrocaudal middle level (Fig. 4D and E).

The number of labeled neurons in the GPi was greater after F2c injection than after F2r injection. The actual number in the F2c injection case was 392 on average (261 cells in Bei and 523 cells in Chi), whereas that in the F2r injection case was 68 on average (102 cells in 06–23 and 33 cells in Hyu). To examine the extent of the area of the two-dimensional density map over which labeled neurons were distributed (Fig. 4), we calculated the proportion of the total bins in the GPi accounted for by bins containing labeled neurons. After F2c injection, the proportion of labeled bins reached as high as 47% on average (122 of 374 bins in Bei, and 185 of 281 bins in Chi; Fig. 4B and C). After F2r injection, in contrast, the proportion of labeled bins was only 12% on average (24 of 370 bins in Hyu, and 58 of 340 bins in 06–23; Fig. 4D and E). These data indicated that labeled neurons in the GPi were distributed four times more widely after the F2c injection than after the F2r injection.

SNr

F2c and F2r injections resulted in different distributions of labeled neurons in the SNr (Fig. 5). To examine the distribution of labeled neurons, we constructed two-dimensional density maps of the SNr (Fig. 6A). After F2c injection, labeled neurons in the SNr were found in the central part through the caudal half of the SNr (Fig. 6B and C). After F2r injection, in contrast, labeled neurons were distributed primarily throughout the rostral half of the SNr (Fig. 6D and E). On average, 64 (36 cells in Bei and 91 cells in Chi) and 36 (44 cells in 06–23 and 28 cells in Hyu) neurons were labeled after F2c and F2r injection, respectively. The proportion of labeled bins was 17% on average (31 of 259 bins in Bei, and 66 of 296 bins in Chi) after F2c injection (Fig. 6B and C), and the proportion of labeled bins after F2r injection was 8% on average (39 of 369 bins in 06–23, and 26 of 409 bins in Hyu; Fig. 6D and E). These results indicated that the origins of multisynaptic projections to F2c and F2r were segregated in the SNr, although the densities of these projections were similar.

Origins of projections to F2c and F2r from the non-output nuclei of the BG

By extending the post-injection survival period up to 4 days, we detected labeled neurons in the GPe, STN, and striatum.

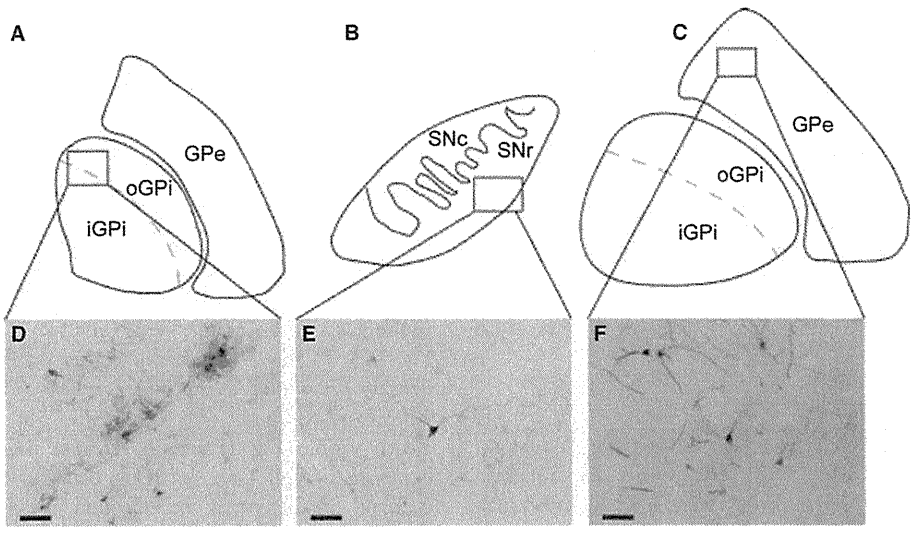

FIG. 2. Neuronal labeling in the GPi and SNr. Second-order neuron labeling in the GPi (A and D) and SNr (B and E) 3 days after the rabies injection into F2. (C and F) Third-order neuron labeling in the GPe 4 days after the rabies injection into F2. The boxed region in A–C is enlarged in D–F. Scale bars in D–F: 50 μm. oGPi, outer portion of GPi; iGPi, inner portion of GPi; SNc, substantia nigra pars compacta.